Atmospheric
Chemistry
and Physics
Discussions

Open Access

Hygroscopic properties of organic aerosol particles emitted in the marine atmosphere

A. Wonaschütz[1], M. Coggon[2], A. Sorooshian[3,4], R. Modini[5,*], A. A. Frossard[5], L. Ahlm[5,**], J. Mülmenstädt[5], G. C. Roberts[5,6], L. M. Russell[5], S. Dey[7], F. J. Brechtel[7], and J. H. Seinfeld[2]

[1]University of Vienna, Faculty of Physics, Vienna, Austria
[2]Department of Chemical Engineering, California Institute of Technology, Pasadena, California, USA
[3]Department of Chemical and Environmental Engineering, University of Arizona, Tucson, AZ, USA
[4]Department of Atmospheric Sciences, University of Arizona, Tucson, AZ, USA
[5]Scripps Institution of Oceanography, University of California, San Diego, CA, USA
[6]Centre National de la Recherche Scientifique – Groupe d'études de l'Atmosphère Météorologique, Toulouse, France
[7]Brechtel Manufacturing, Inc., Hayward, CA, USA
[*]now at: Ecole Polytechnique Federale de Lausanne, Lausanne, Switzerland
[**]now at: Department of Applied Environmental Science, Stockholm University, Stockholm, Sweden

Discussion Paper | Discussion Paper | Discussion Paper | Discussion Paper

ACPD
13, 11919–11969, 2013

Emitted organic plume

A. Wonaschütz et al.

Title Page

Abstract | Introduction

Conclusions | References

Tables | Figures

|◄ | ►|

◄ | ►

Back | Close

Full Screen / Esc

Printer-friendly Version

Interactive Discussion

Correspondence to: A. Sorooshian (armin@email.arizona.edu)

Emitted organic plume

A. Wonaschütz et al.

Title Page

Abstract | Introduction

Conclusions | References

Tables | Figures

◄ | ►

◄ | ►

Back | Close

Full Screen / Esc

Printer-friendly Version

Interactive Discussion

Abstract

During the Eastern Pacific Emitted Aerosol Cloud Experiment (E-PEACE), a plume of organic aerosol was produced and emitted into the marine atmosphere from aboard the research vessel R/V *Point Sur*. In this study, the hygroscopic properties and the chemical composition of the plume were studied at plume ages between 0 and 4 h in different meteorological conditions. In sunny conditions, hygroscopic growth factors (GFs) at a relative humidity (RH) of 92 % were low, but increased at higher plume ages: from 1.05 to 1.09 for 30 nm and from 1.05 to 1.1 for 150 nm dry size (contrasted by an average marine background GF of 1.6). Simultaneously, ratios of oxygen to carbon (O : C) increased from < 0.001 to 0.2, water-soluble organic mass (WSOM) concentrations increased from 2.42 to 4.96 $\mu g\,m^{-3}$, and organic mass fractions decreased slightly (~ 0.97 to ~ 0.94). New particles were produced in large quantities (several $10\,000\,cm^{-3}$), which lead to substantially increased cloud condensation nuclei (CCN) concentrations at supersaturations between 0.07–0.88 %. High-resolution aerosol mass spectrometer (AMS) spectra show that the organic fragment m/z 43 was dominated by $C_2H_3O^+$ in the small particle mode and by $C_3H_7^+$ in the large particle mode. In the marine background aerosol, GFs for 150 nm particles at 40 % RH were found to be enhanced at higher organic mass fractions. An average GF of 1.06 was observed for aerosols with an organic mass fraction of 0.53, a GF of 1.04 for an organic mass fraction of 0.35.

1 Introduction

The interaction of atmospheric aerosol particles with water is a crucial factor affecting their evolution in the atmosphere. By taking up water, particles grow in size and experience modifications to their refractive index, which changes their ability to interact with solar radiation. Activation into cloud drops is a determining factor in the atmospheric lifetime of particles. Furthermore, cloud droplets and water in deliquesced

Title Page

Abstract | Introduction

Conclusions | References

Tables | Figures

◀ | ▶

◀ | ▶

Back | Close

Full Screen / Esc

Printer-friendly Version

Interactive Discussion

aerosol particles provide an aqueous medium for chemical reactions, which can lead to a change in the chemical composition of the particles (Hegg, 1985; Blando and Turpin, 2000; El Haddad et al., 2009; Bateman et al., 2011; Ervens et al., 2011).

Organic compounds can have a profound impact on the water-uptake properties of particles. An increase in the organic mass fraction in aerosol particles can reduce water uptake at relative humidities (RH) above the deliquescence RH (DRH) of salts, while simultaneously enabling hygroscopic growth at RHs below the DRH (e.g., Dick et al., 2000; Hersey et al., 2009; Meyer et al., 2009). In the atmosphere, aging processes affect hygroscopic properties of the organic fraction of aerosols (commonly referred to as organic aerosols, OA). Organic components in fresh aerosols have been observed to decrease water uptake, but in aged aerosols, they can have the opposite effect (Saxena et al., 1995). Aging of aerosols broadly encompasses any changes in their chemical composition and physical properties during their lifetime in the atmosphere. For OA, important aging processes include the addition of organic mass through secondary production via gas-to-particle conversion and aqueous-phase production (e.g., George et al., 2007; El Haddad et al., 2009; Ervens et al., 2011), and the continuing oxidation during photochemical and cloud processing (Jimenez et al., 2009). The transition from less oxidized to more oxidized organic compounds in OA increases hygroscopic growth factors (GF = $d_{p,RH}/d_{p,dry}$) (Massoli et al., 2010; Duplissy et al., 2011). The conversion of hydrophobic primary OA to hydrophilic particles has been shown to be rapid during the daytime in an urban environment (Wang et al., 2010).

Hygroscopic growth and cloud condensation nuclei (CCN) activity are often described in terms of a single parameter connecting the hygroscopicity of particles in the sub- and the super-saturated regime (Petters and Kreidenweis, 2007; Wex et al., 2008; Dusek et al., 2011). However, observations of several aerosol types, including biomass burning aerosol (Petters et al., 2009; Dusek et al., 2011), laboratory-generated secondary organic aerosol (SOA) (Wex et al., 2009), primary marine organic aerosol (Ovadnevaite et al., 2011a) and urban ambient aerosol (Hersey et al., 2013), have shown conflicting behavior in the form of reduced hygroscopic growth factors with

simultaneous enhancements in CCN activity. The role of organic compounds in changing water-uptake properties of aerosols is not fully understood.

The marine environment is well suited to study the aging of organic aerosols. In continental locations, with numerous anthropogenic and natural aerosol sources, fresh

5 and aged organic aerosols are often found in the same air mass. Over the ocean, in contrast, sources of organic aerosols are more limited. Continental outflow is often the most important source of OA (Hawkins et al., 2010), however, primary and secondary marine sources can be relevant (Gantt and Meskhidze, 2012). An important marine primary organic aerosol source is bubble-bursting, which transfers dissolved or

10 film-forming organic substances from the ocean surface into the particle phase in the atmosphere (e.g., Middlebrook et al., 1998; O'Dowd et al., 2004; Cavalli et al., 2004; Leck and Bigg, 2005; Facchini et al., 2008a; Russell et al., 2010; Ovadnevaite et al., 2011b). Proposed marine sources of SOA include biogenic amines (Facchini et al., 2008b; Sorooshian et al., 2009; Dall'Osto et al., 2012), isoprene oxidation above phy-

15 toplankton blooms (Meskhidze and Nenes, 2006; O'Dowd and de Leeuw, 2007), and aqueous-phase production in marine stratus clouds (Crahan et al., 2004; Sorooshian et al., 2010). In the absence of such sources, marine background aerosol typically shows a hygroscopic mode with growth factors around 1.6–1.79 at 90 % RH (Swietlicki et al., 2008 and references therein). Less hygroscopic and hydrophobic modes are en-

20 countered in continental outflow (e.g., Hawkins et al., 2010; Hegg et al., 2010), free tropospheric air masses, and during episodes of fresh biogenic aerosol production (Swietlicki et al., 2008; Allan et al., 2009; Hersey et al., 2009; Mochida et al., 2011). Hygroscopic growth factors and the activation ratio (the ratio of CCN at a given supersaturation to the total measured particle number concentration, CCN/CN) have been

25 shown to increase with the age of the continental air mass (Massling et al., 2007; Furutani et al., 2008). Anthropogenic disturbances such as emissions from ship traffic and oil spills constitute further sources of organic aerosols in the marine atmosphere. The injection of container ship exhaust, which includes particles consisting of a mix of hydrocarbon-like organic aerosol and sulfate (Murphy et al., 2009), is a persistent

anthropogenic impact on atmospheric composition (Eyring et al., 2009). During the Deepwater Horizon oil spill, hydrocarbon-like SOA was found to derive from intermediate volatility organic compounds evaporated from the oil surface (de Gouw et al., 2011). Most of these particles acted as CCN at supersaturations exceeding 0.3 %, but were
5 characterized by low hygroscopicity in the sub-saturated regime (Moore et al., 2012).

This study aims to improve the process-level understanding of changes in water-uptake properties of organic aerosol by investigating a rare "hybrid experiment" between laboratory and field conditions: a well-defined organic aerosol is artificially generated in large quantities and exposed to the real atmosphere. We report measurements
10 of hygroscopic growth factors and CCN concentrations in this organic plume injected into the marine atmosphere, and compare the aging of the plume and its hygroscopic properties in both cloudy and sunny conditions.

2 Methods

2.1 The E-PEACE field campaign

15 The Eastern Pacific Emitted Aerosol Cloud Experiment (E-PEACE) was a field campaign conducted off the coast of California in July and August of 2011. Its general aim was to study aerosol-cloud-radiation interactions through the controlled emission of known aerosols into the marine stratocumulus deck and the measurement of their effects from ship, aircraft and satellite observational platforms. A detailed description
20 of the experiment and its first results are given by Russell et al. (2013). The location of the experiment is shown in Fig. 1. In this study, we investigate an organic plume produced on and emitted from the Research Vessel (R/V) *Point Sur* on a 12 day research cruise (12–23 July). To create the plume, a paraffin-type oil was vaporized into a thick smoke (organic plume) (Russell et al., 2013) using smoke generators at the
25 ship's stern (Fig. 1). The properties of the organic plume and its interactions with the marine environment were measured from two platforms: the Center for Interdisciplinary

Remotely-Piloted Aircraft Studies (CIRPAS) Twin Otter aircraft and an instrument container on the R/V *Point Sur* itself. This study focuses on measurements from the R/V *Point Sur*.

2.2 Instruments

A complete list of all instruments located on the two platforms is given by Russell et al. (2013). The instruments onboard the R/V *Point Sur* whose data are used for this study are summarized in Table 1. The R/V *Point Sur* instrument container was located at the ship's bow. A common vertical inlet, which was shielded from spray, sampled ambient aerosol up to several micrometers in diameter. The aerosol was dried in diffusion driers before distribution to the instruments. Sub-micrometer particle size distributions were measured with a Scanning Electrical Mobility Spectrometer (SEMS Model 138 2002, Brechtel Manufacturing Inc.). Size distributions of larger particles were measured with an Aerodynamic Particle Sizer (APS 3321, TSI Inc., size range 0.5–20 µm) and an Optical Particle Sizer (OPS 330, TSI Inc., size range 0.3–10 µm). A condensation particle counter (CPC 3010, TSI Inc.) measured total particle number concentration.

Hygroscopic growth factors were measured using a Humidified Tandem Differential Mobility Analyzer (HTDMA Model 3002, Brechtel Manufacturing Inc.) (Sorooshian et al., 2012). The system consisted of a dry DMA (DMA 1, RH < 8 %) selecting particles with dry diameters of 30, 75, 150 and 300 nm, a humidifier, in which the dry particles were exposed to RHs of 40, 70, 85 and 92 %, and a second, humidified DMA (DMA 2), which measured the number size distribution after hygroscopic growth. CCN concentrations for supersaturations (S) ranging between 0.07–0.88 % were measured using a CCN counter (custom design, miniaturized after Roberts and Nenes, 2005).

Sub-micrometer particles, separated from larger particles with a cyclone, were analyzed with a High Resolution Time-of-Flight Aerosol Mass Spectrometer (AMS, Aerodyne Research Inc.) (DeCarlo et al., 2006) to measure the non-refractory, inorganic (ammonium, sulfate, nitrate, chloride) and organic chemical composition.

Sub-micrometer particles were also collected on 37 mm Teflon filters and scanned using Fourier transform infrared (FTIR) spectroscopy (Tensor 27, Bruker Optics, Inc.) (Russell et al., 2009; Frossard and Russell, 2012). Samples of the ship diesel and smoke oil that were used during E-PEACE cruise were atomized (atomizer, TSI Inc.), collected on Teflon filters, and scanned using FTIR spectroscopy.

Water soluble organic carbon (WSOC) was quantified in sub-micrometer particles with a Particle-Into-Liquid Sampler (PILS, Brechtel Manufacturing Inc.) coupled to a total organic carbon analyzer (Sievers, Model 800) (Sullivan et al., 2006; Wonaschuetz et al., 2011). Black carbon (BC) concentrations were obtained from a Single Particle Soot Photometer (SP2, Droplet Measurement Technologies Inc.). Meteorological conditions, including ambient temperature, wind direction and speed (corrected for the ship's movement), and RH were measured routinely on the R/V *Point Sur*, along with ship-specific data such as heading and speed. Additional visual observations (e.g., fog, other ships) were noted in deck logs.

Mass concentrations of oxalate and glyoxylate are reported for the smoke sampling events (described in Sect. 2.6). PM_{10} was collected on pre-baked 47 mm quartz fiber filters that were stored in a freezer prior to chemical analysis. The filter extraction procedure consisted of ultrasonication (15 min) of filter halves with 18.2 MΩ Milli-Q water. Syringe filters (Acrodisc filter, 25 µm) were used to remove any remaining insoluble matter from the extracts after ultrasonication. Ion chromatography analysis (IC; Thermo Scientific Dionex ICS-5000 anion system with an AS11-HC 2 mm column) was conducted using a 38 min multi-step gradient program with sodium hydroxide eluent (1 mM from 0 to 8 min, 1 mM to 30 mM from 8 to 28 min, 30 mM to 60 mM from 28 to 38 min).

2.3 Data processing and quality control

For the HTDMA data, an important source of uncertainty is the variability of RH in DMA 2 (Swietlicki et al., 2008). For quality control, the RH in DMA 2 and its variability in time (over the duration of a scan) and space (along the DMA 2 column) were calculated from flow rates, temperatures, and measured RH in the sample flow out of the humidifier and

Title Page

Abstract   Introduction

Conclusions   References

Tables   Figures

◄   ►I

◄   ►

Back   Close

Full Screen / Esc

Printer-friendly Version

Interactive Discussion

in the sheath flow in DMA 2 at the beginning of the DMA 2 column (these two flows were humidified separately), and of temperature in the excess flow at the end of the DMA 2 column. Scans were accepted if they fulfilled the following criteria: (i) flow rates were within 25 % of the set point; (ii) combined humidifier and sheath air RH variability over the time of a scan did not exceed ±1.5 % RH; and (iii) the temperature gradient over the length of the DMA 2 did not exceed ±1°C. The raw count data from DMA 2 were inverted to produce the growth factor distributions: raw counts were shifted in time to correct for particle transit time between the DMA column and particle counter and de-smeared to correct for a finite particle counter response time. The de-smeared data were finally inverted using the diffusing form of the DMA transfer function (Stolzenburg, 1988) and assuming a single charge. Correcting only for a single charge (i.e., inverting for DMA 2 only, rather than the combined TDMA system) will accurately recover GF values and the relative fractions of growth factor populations, with some limitations on the resolution of the distribution shape (Gysel et al., 2009). Growth factors were estimated by fitting a lognormal function to the growth factor distributions, assuming mono-modal distributions as a first order estimate and advancing to multi-fit peaks when needed (Sect. 3.4).

The SEMS, OPS and APS each use a different operating principle to size aerosol particles. Total aerosol size distributions were created by merging distributions over the nominal diameter range 0.01–20 µm using an algorithm based on Khlystov et al. (2004). For the AMS data, a collection efficiency of 0.5 and a detection limit of 0.01 µg m^{-3} were applied. Total non-refractory mass concentrations were calculated as the sum of organic and inorganic concentrations. Size distributions of the non-refractory mass components were calculated from the AMS measurements (DeCarlo et al., 2004, 2006). Since the measured masses were close to the detection limit, the size distributions were smoothed over 11 size bins, corresponding to diameter intervals between 21 nm (midpoint: 20 nm) and 266 nm (midpoint: 946 nm). The AMS V-mode measurements were used to calculate the ratio of oxygen to carbon (O : C) in the measured organic particles (Aiken et al., 2007). For the WSOC measurements, the detection limit was

0.1 µg C m^{-3}. WSOC concentrations were converted into water-soluble organic matter (WSOM) concentrations using two different conversion factors based on literature values (Turpin and Lim, 2001): 1.4 for the R/V *Point Sur* organic plume, and 1.8 for the marine background aerosol. Water-insoluble organic matter (WIOM) was calculated as

5 the difference between AMS organic and WSOM. The FTIR functional group composition was determined using an automated algorithm that includes baselining, peak-fitting, and integrating at specific wavenumbers associated with major carbon bond types (Russell et al., 2009; Takahama et al., 2012). The functional groups that were quantified include hydroxyl, alkane, amine, carbonyl, and carboxylic acid groups.

10 **2.4 Auxiliary data**

Three-day HYSPLIT back-trajectories (Draxler and Rolph, 2012) ending at the ship's location and at an altitude of 50 m were calculated for every third hour of the R/V *Point Sur* cruise. GOES visible satellite images (every 15 min) were collected and overlaid onto plots of the R/V *Point Sur* track to confirm and complement the visual observations

15 of clouds from the R/V *Point Sur*. To analyze synoptic weather conditions, maps of surface temperature, wind, pressure, and 500 mb geopotential height were obtained from the website of the NOAA/OAR/ESRL Physical Science Division (http://www.esrl.noaa.gov/psd/data/composites/day/).

2.5 Synoptic conditions

20 Synoptic conditions during the cruise were characterized by two different regimes, as determined by the 500 mb geopotential height charts: the first ("Regime 1", 12–19 July) was governed by a mid-latitude trough north of the cruise region; the second ("Regime 2", 20–23 July) was characterized by the re-establishment of a seasonally typical subtropical ridge to the south. Regime 1 was characterized by lower surface temperatures.

25 HYSPLIT back-trajectories show that during Regime 1, air masses arrived from the NW (Fig. 2). During the regime change (18–19 July), hereinafter termed "Transition",

an episode of back-trajectories from the west is apparent, in conjunction with a surface low-pressure center just north of the cruise area. Back-trajectories parallel to the coast were dominant during Regime 2.

2.6 Plume tracking

During the majority of the cruise, ambient background aerosol was measured. Background measurements are defined as time periods with CPC particle number concentrations $< 1000\,\text{cm}^{-3}$. On several occasions the R/V *Point Sur* turned into the freshly generated plume and tracked it downwind. Plume tracking was limited by the ship's maximum speed, which was slower than typical wind speeds on most days. The ship was able to catch up with and track the plume on three days (16, 17 and 18 July, green shading in Fig. 3). The plume was tracked both by visually following the plume and by monitoring CPC particle number concentrations in real time. The ship's course was changed when needed to follow the highest concentrations. For this study, the two plume tracking periods on 17 and 18 July were chosen for comparison. Plume characterization thus took place in air masses that were less influenced by coastal air (Regime 1 and Transition). The R/V *Point Sur* stack exhaust was sampled on one occasion on 22 July (yellow shading in Fig. 3).

17 July was one of only two cloud-free days during the R/V *Point Sur* cruise (Fig. 3, panel 3). GOES visible images show that clouds were present in the early morning but started to dissipate around 10:00 local time (LT, which is used hereinafter). The general area around the R/V *Point Sur's* location was cloud free by 13:00. Relative humidity dropped from 91 % around sunrise (05:54) to 80 % at noon and further to an all-cruise minimum of 70 % by 18:00. Ambient temperature in the same time frame ranged between 13.6 and 15.7 °C. Smoke production on the R/V *Point Sur* began at 06:45 and ended at 11:15. The wind direction measured on the R/V *Point Sur* during smoke production and tracking was between 300° and 350°, with an average wind speed of $3.7 \pm 0.9\,\text{m s}^{-1}$. The low wind speed on 17 July allowed plume tracking by the R/V *Point Sur* for several hours. Figure 4a shows the ship track as the plume was

sampled. Smoke properties were measured during the time periods 11:20–11:32 (A1, fresh plume), 11:36–13:10 (A2, somewhat aged plume), and 15:02–15:39 (A3, aged plume). The plume was also encountered between 13:20 and 14:00, but it is likely that sampling occurred at the edge rather than at the center of the plume. Therefore, this time period was not included in this analysis. The age of the plume encountered during tracking was estimated using the average wind speed and calculating the transport time from the location of the last smoke production to the ship's locations during the three time periods of plume sampling. This estimate of plume age represents a lower boundary as the smoke encountered at a particular point may have been produced at a time earlier than the last smoke production. The lower bounds of the plume ages during the three time periods of interest were estimated to be A1 $\approx$ 6 min, A2 $\approx$ 1.6 h and A3 $\approx$ 4.2 h.

On 18 July, it remained cloudy throughout the day. In addition, thick fog was noted in the deck logs (the ship's fog horn was used) from 04:00 to noon. RH remained close to 100 % during most of the morning and only dropped below 95 % at 12:25. Ambient temperature ranged between 14.6 and 16.4 °C. The R/V *Point Sur* track during smoke sampling is shown in Fig. 4b. Smoke was produced in two stages, from 06:45 to 07:40 and again from 09:00 to 09:30. Intermittent smoke sampling at the plume's edge occurred between 06:15 and 08:30. The center of the plume was tracked successfully between 09:35 and 10:45. The typical wind speed during smoke production and plume tracking was $5.4 \pm 1.3 \, \mathrm{m \, s^{-1}}$, with a direction between 190–240°. The estimated plume ages were A1 $\approx$ 2 min and A2 $\approx$ 37 min.

During the plume tracking events (green shading in Fig. 3), the organic mass fraction in the fresh plume (plume age A1) was $\geq$ 97 %, as also found by Russell et al. (2013). The primary plume particles were created at a rate of 10^{11}–$10^{13} \, \mathrm{s^{-1}}$, and ranged between 100 nm and 8 µm in diameter (Russell et al., 2013). The high organic mass fraction distinguished the plume from other cargo ship exhaust plumes, which typically contain $\sim$ 50 % sulfate (Russell et al., 2013), and from the background marine aerosol, which was found to contain between 40 and 60 % organic mass. The average ratio of

Emitted organic plume

A. Wonaschütz et al.

Title Page

Abstract	Introduction
Conclusions	References
Tables	Figures

|◄ | ►|

◄ | ►

Back | Close

Full Screen / Esc

Printer-friendly Version

Interactive Discussion

organic:sulfate mass encountered in the background aerosol was 1.15 ± 0.80 and exceeded 5.0 in only a couple measurements during the entire campaign. Therefore, the plume was identified through AMS measurements for which the ratio of organic:sulfate exceeded 5. R/V *Point Sur* stack emissions (yellow shading in Fig. 3) also had very high organic mass fractions (around 90–95 %), but were characterized by higher BC concentrations ($> 6\,\mathrm{ng\,m^{-3}}$) and lower overall mass concentrations. Using BC as an indicator, we find that stack emissions influenced the plume measurements only on rare occasions. For both plume sampling events, the total volume concentrations of the plume during tracking (A2) were comparable (see also Fig. 11), suggesting that the attempt to track the center of the plume was successful.

3   Results

3.1   Background aerosol

The background aerosol was dominated by sulfate and organic (Fig. 3). Air masses in Regime 2 (back-trajectories parallel to the coast) are characterized by higher overall concentrations of accumulation mode particles (panel 1), BC (panel 2) and ammonium (panel 4). The average background BC concentration during Regime 1 was $1.03 \pm 1.06\,\mathrm{ng\,m^{-3}}$, while the average during Regime 2 was higher at $1.8 \pm 1.01\,\mathrm{ng\,m^{-3}}$ (statistically significant difference at 99 % confidence level), indicative of more anthropogenic influence during the latter period. For comparison, BC concentrations documented in urban atmospheres including Los Angeles, Mexico City, and Santiago, Chile, range from 0.002–$75\,\mathrm{\mu g\,m^{-3}}$ (Metcalf et al., 2012 and references therein). Short spikes in BC concentrations were observed in both regimes, and confirm that the aerosol encountered during Regime 1 was still far from pristine. This is consistent with other work in the region showing that the regional aerosol is persistently influenced by anthropogenic sources (Hegg et al., 2010; Coggon et al., 2012). During Regime 2, wind speeds typically ranged between 5 and $15\,\mathrm{m\,s^{-1}}$, a range in which externally mixed sea

salt starts to be an important contributor to the ambient aerosol (Swietlicki et al., 2008 and references therein). Higher concentrations of particle volume in the 400 nm–1 μm range (Fig. 3, top panel) may therefore have their origin in bubble bursting processes. Ammonium contributed on average $0.04 \pm 0.02\,\mu\mathrm{g\,m}^{-3}$ to the total detected AMS mass in Regime 1, and $0.08 \pm 0.02\,\mu\mathrm{g\,m}^{-3}$ in Regime 2. A link between aerosol chemistry and biological emissions in coastal waters, which are a source of ammonium, was established for the same region by Sorooshian et al. (2009).

Hygroscopic growth factors at lower RH (40 % and 70 %), below the deliquescence RH of most common inorganic salts, differed by meteorological regime. Table 2 shows that for a particle dry size of 150 nm, the growth factors averaged over Regime 2 were significantly lower (95 % confidence level in a two-sample z-test) than those averaged over Regime 1. The growth at a RH below the deliquescence RH of most inorganic salts is at least partly enabled by the presence of organics (e.g., Hersey et al., 2009). It is unlikely that previous hygroscopic growth of inorganic components caused the observed growth as the aerosol was dried to RH < 8 % before growth factor measurement, well below the efflorescence RH of most common salts. The lower growth factors observed in Regime 2 at 40 and 70 % RH could be caused by the higher BC concentrations (if internally mixed) and/or by a lower organic mass fraction: the average sub-micrometer organic mass fraction was 0.53 ± 0.11 in Regime 1 and 0.35 ± 0.10 in Regime 2. Additionally, the organic fraction in Regime 1, with trajectories from the sea rather than from coastal regions, may be more aged and therefore more hygroscopic. At a RH above the deliquescence of pure salts (92 % and 85 %), there was no significant difference in growth factors between Regimes 1 and 2. In previous campaigns, lower growth factors at high RH have been observed in continentally-influenced air masses, referring to back-trajectories originating over the continent (e.g., Massling et al., 2007; Allan et al., 2009; Hersey et al., 2009). This type of back-trajectory was not encountered during this campaign (Fig. 2), explaining the lack of a more striking difference in growth factors by air mass origin at higher RH. Over the entire campaign, growth factors at 92 % RH (particle dry diameter of 150 nm) ranged between 1.43 and 1.96, with an average of

1.64 ± 0.11. These values compare well with the "more hygroscopic modes" observed in marine accumulation mode aerosol in other studies (Massling et al., 2007; Swietlicki et al., 2008 and references therein; Allan et al., 2009; Mochida et al., 2011), and are associated with internally mixed aerosols containing sulfate, aged sea salt and organic matter (Swietlicki et al., 2008). Higher growth factors are expected for fresh/pure sea-salt particles and were found in the background aerosol of 18 July (Sect. 3.4).

3.2 Secondary organic aerosol formation in the plume

The most striking difference between the two plume tracking events (17 July, sunny, and 18 July, foggy) can be seen in the particle number concentrations in the aged plume (black/white marker boundaries in Fig. 4). On 18 July (Fig. 4b), number concentrations initially showed a short spike of $30\,000\,cm^{-3}$, but dropped below $5000\,cm^{-3}$ within five minutes and soon approached levels only about 40 % above the background. On 17 July (Fig. 4a), in contrast, particle number concentrations of several $10\,000\,cm^{-3}$ were observed for several hours at ages A2 and A3. These high particle concentrations, hours after the plume production stopped, cannot arise from the emitted primary particles and are consistent with new particle formation successfully competing with dilution and coagulation. The temporal coincidence of these high number concentrations with the chemical signature of the plume (organic : sulfate > 5) and the absence of comparably high concentrations at any other time during the cruise make it highly unlikely that the particles derived from any source other than the R/V *Point Sur* plume.

Figure 5 shows number and volume distributions for the plume sampling events measured by the DMA (10–500 nm) and the merged APS/OPS data (500 nm–2 µm). On 17 July, a "banana plot" typical of new particle formation and subsequent growth, is visible from 11:36 to 13:10 (Fig. 5a, age A2). Given the composition of the fresh plume (Sect. 2.6), it is likely that volatile organic compounds (VOCs) were also emitted in the gas phase, along with the primary particles from the generators. The VOCs may have condensed after dilution and cooling, or underwent oxidation to form SOA in the aging plume. SOA formation can be accompanied by nucleation of particles (dall'Osto et al.,

2012). Alternatively, VOCs may have evaporated from primary plume particles, and formed SOA after photo-oxidation, in a process similar to that shown in the laboratory chamber experiments by Robinson et al. (2007). Figure 5c shows initial plume particles in a size range of 500 nm–1 µm approximately 5 min before the onset of new particle formation, and a subsequent decrease of both total volume and the mode of the volume distribution. This is an indicator of evaporation of plume particles, which then could have produced the VOCs necessary for small particle nucleation and growth.

A similar development potentially signifying evaporation of primary plume particles is also visible on 18 July (Fig. 5d). However, no new particle formation and growth was observed. It is conceivable that different locations within the plume may have different particle size characteristics, and that different parts of the plume may have been sampled on the different days. Due to variable wind speeds and reduced visibility on the foggy 18 July, it was difficult to follow the plume in an identical manner on both days. The higher concentrations of large particles observed on 18 July indicate that at least initially, a somewhat denser and fresher part of the plume (compared to the fresh plume on 17 July) was sampled. However, the plume was produced identically on both days, and, as described in Sect. 2.6, care was taken to follow the highest particle number concentrations. The most striking differences distinguishing 18 July from 17 July were the presence of fog and the diminished solar radiation due to clouds and fog (Fig. 3, middle panel). There are at least two explanations for the absence of a nucleation and growth event: (i) VOCs may have partitioned onto existing surfaces (e.g. fog droplets) instead of forming new particles – at least parts of the plume were able to enter the liquid phase as evidenced by observations of the organic signature of the plume in cloud droplet residual particles (Shingler et al., 2012); and (ii) if photo-oxidation of plume VOCs was responsible for SOA formation on 17 July, cloud and fog shading may have suppressed such processes on 18 July.

3.3 CCN concentrations

The temporal development of CCN concentrations and activation ratios during the plume sampling periods is shown in Fig. 6. On both days, CCN concentrations at the lower supersaturation (S) of 0.07–0.08 % are largely unaffected by the presence of the plume. At medium ($0.24 < S < 0.26$ %) and high ($0.87 < S < 0.88$ %) S, a substantial number of particles activated. On 17 July (Fig. 6a), the onset of new particle formation at 11:32 was accompanied by a dramatic reduction in the activation ratio. The use of the CCN activation ratio as a proxy for hygroscopicity requires caution when there is a high variability in the aerosol size distribution, as is clearly the case here: the drop in activation ratios is a result of the order of magnitude increase in condensation nuclei (CN) concentrations between A1 and A2. As the plume ages, CCN concentrations increase and eventually reach over 4000 cm^{-3} at high S. Changes in the size distribution are often the primary driver for CCN concentrations (Roberts et al., 2002; McFiggans et al., 2006), and probably explain most of the increase in the CCN concentrations at the high S observed here: the newly-formed particles are too small to act as CCN, but grow into the relevant size ranges (Fig. 6a, A2, after 12:00) as the plume ages. At plume age A3, particles have grown into the accumulation mode (Fig. 5a) and CCN concentrations reach 637 and 9910 cm^{-3} at the medium and high S, respectively. In agreement with previous findings (Hennigan et al., 2012), new SOA particle formation can contribute a substantial number of new CCN. An interesting aspect is that at plume age A2, absolute CCN concentrations at the medium S increase (from 138 cm^{-3} at 11:24 to 294 cm^{-3} at 12:10) before they do at the high S. This indicates that as the plume aged, not only did the newly-formed particles start to act as CCN as they grew into the respective size range – this would be visible as increased CCN concentrations at higher S first – but likely some of the primary plume particles became more hygroscopic and started to activate.

On 18 July (Fig. 6b), activation ratios were only initially suppressed, and increased steadily as CN concentrations decreased. The absolute CCN concentration at high

S increased with increasing plume age, from 151 cm^{-3} at 09:33 to a peak value of 424 cm^{-3} at 10:13, a far lower concentration than on 17 July. Since there was no such dramatic change in the size distribution as on 17 July, the increase in CCN concentration on 18 July was likely driven by chemical changes of the existing particles.

The activation diameter for medium and high S was estimated by integrating the merged APS/OPS and DMA size distributions from the largest to smaller sizes to match the observed CCN concentrations. On 17 July, the estimated activation diameter (d_{act}) was smaller than the Kelvin diameter (d_K) at both of the higher supersaturations ($d_K =$ 0.81 µm for $S = 0.26\%$ and $d_K = 0.24$ µm for $S = 0.88\%$) and at all plume ages. This implies that plume particles smaller than the Kelvin diameter activated, due to the probable presence of soluble ions and a certain degree of hygroscopicity. On 18 July, the estimated activation diameter was larger than the Kelvin diameter for both supersaturations at age A1. For medium S, d_{act} was lower than d_K at plume age A2; for high S, d_{act} stayed above d_K. An activation diameter larger than the Kelvin diameter can occur if a sub-population of particles does not activate even at high S. Instances of $d_{\text{act}} > d_K$ thus point to the presence of an external mixture (Burkart et al., 2012). As discussed in Sect. 3.2, a fresher part of the plume was likely sampled on 18 July. Thus, the external mixture may comprise both large plume particles that did not activate, and more aged plume particles, which activated at a size below d_K. Bulk measurements of CCN in externally mixed aerosols are prone to uncertainties, thus, future work should aim to measure size-resolved CCN concentrations. A decreasing trend in estimated d_{act} was observed at both supersaturations and on both days, and is indicative of a chemical transformation of CCN-inactive to CCN-active particles (e.g., Furutani et al., 2008).

As reported by Russell et al. (2013), the amount of CCN created in the plume was sufficient to create a ship track in the marine stratocumulus deck that was visible via satellite remote sensing. The primary plume particles were large enough to activate without the presence of soluble ions (Russell et al., 2013). Supersaturations in the stratocumulus deck are generally estimated to be in the range of 0.1–0.4 % (Hoppel et al., 1996; Feingold et al., 1998; Thouron et al., 2012). During E-PEACE, in-cloud

Title Page

Abstract | Introduction

Conclusions | References

Tables | Figures

|◄ | ►|

◄ | ►

Back | Close

Full Screen / Esc

Printer-friendly Version

Interactive Discussion

supersaturations of 0.09 and 0.25 were estimated during two Twin Otter flights on 16 July and 10 August (Russell et al., 2013). Based on these findings, it is possible that some of the newly-formed particles can act as CCN as well.

3.4 Hygroscopic growth factors

Given the CCN activity of the plume particles described above, the question arises as to what extent specific trends are mirrored in the hygroscopic growth data for the sub-saturated regime. Hygroscopic growth factors (92 % RH) measured in the plume on 17 July at age A2 and A3 (Fig. 6a) are low: for particles with a dry size of 30 nm (representative of the newly-formed particles), GFs range between 1.05 and 1.09. Those with a dry size of 150 nm (representative of larger plume particles) show GFs increasing from 1.02 to 1.10. The high GFs measured at the very beginning and the very end of the plume period are representative of background marine aerosol, as evidenced by the low number concentrations in the respective GF distributions (about a factor of two lower than those observed in the "thick of the plume"). Particles with a dry size of 75 nm did not grow at any plume age. The 75 nm particles are representative of the particles contributing most to the CCN concentrations, as the particle number concentration in the plume is dominated by particles in the size range below 100 nm (Fig. 5a).

On 18 July, in contrast, the hygroscopic growth behavior is different: GFs increase with increasing plume age (Fig. 6b). For particles with a dry size of 30 and 75 nm, the GF distributions (not shown) were bimodal, showing a mode with negligible hygroscopic growth and a background mode with GFs between 1.5 and 1.7. For 150 nm particles, the GF distributions were mono-modal, but very broad, suggesting the presence of several overlapping peaks which are not readily distinguishable. In order to gain more insight, the distributions were approximated with a fit of three lognormal modes: in the background aerosol (i.e., an average over all scans of 18 July which were uninfluenced by local particle sources), two higher GF modes were found and yielded GFs of 1.60 and 2.09. One of these modes (GF = 1.60) corresponds to the "more hygroscopic mode" (Sect. 3.1) of the marine background, the other (GF = 2.09) potentially to a pure

Title Page

Abstract | Introduction

Conclusions | References

Tables | Figures

|◄ | ►|

◄ | ►

Back | Close

Full Screen / Esc

Printer-friendly Version

Interactive Discussion

sea salt mode (Swietlicki et al., 2008). These two modes were assumed to be present and invariant throughout plume sampling. With this constraint, a lognormal mode was fit that best explained the remainder of the GF distribution. This mode was still wider than the GF distributions for plume particles observed on 17 July, and thus the possibil-
5 ities that additional modes were present, or that the background during plume tracking may differ from the all-day average, cannot be excluded. The GFs shown in the gray shaded area in Fig. 6b pertain to the modeled lower GF mode. Within eight consecutive scans, the GF increased from 0.94 to 1.47, a much larger increase than on 17 July. While these GF values seem to approach background values, it has to be noted that
10 number concentrations in all GF scans were at least 36 % higher than those in background GF distributions, and organic mass fractions were above 91 % (Fig. 7b), thus sampling occurred well within the plume.

An increase in GF is most easily explained by a shift from a purely organic aerosol to one with more hygroscopic, internally mixed inorganic compounds. Mixing of plume
15 particles with the background aerosol or deposition of sulfate on the plume particles are plausible processes to explain the GF increases on both days. Equally possible is a transformation of the organic fraction to more hygroscopic compounds, as suggested by Jimenez et al. (2009). For the 30 nm particles on 17 July, internal mixing with inorganic compounds is an unlikely process to explain growth, as particles of that size are
20 typically freshly generated and did not have much time in the atmosphere to become internally mixed. Hence, their organic characteristics, rather than their mixing state, should explain the observed growth. Further insight into these possibilities is provided by chemical composition measurements.

3.5 Chemical composition

25 Figure 7 shows the progression of absolute AMS organic and PILS water-soluble organic mass concentrations (top panels), as well as the ratio of O : C and the water-soluble organic fraction (bottom panels) with plume age. The trend towards decreasing overall organic mass in the aging plume is attributable to dilution as the ship moved

farther away from the location of the last smoke production, and potentially also to evaporation of organic mass from primary plume particles (Sect. 3.2).

On 17 July (Fig. 7a), the sustained CPC number concentrations of $> 30\,000\,\mathrm{cm}^{-3}$ designate the time frame in which new particle formation was outbalancing coagulation and dilution. These number concentrations represent a lower limit as the CPC has substantial coincidence errors at concentrations $> 10\,000\,\mathrm{cm}^{-3}$ and does not report values exceeding $40\,000\,\mathrm{cm}^{-3}$; sustained concentrations reflect new particle formation successfully competing with other processes such as dilution and coagulation. An interesting aspect is the increase of absolute concentrations of WSOM from $2.42\,\mathrm{\mu g\,m}^{-3}$ at 11:26 to $4.96\,\mathrm{\mu g\,m}^{-3}$ at 12:32. Since the typical background WSOM concentrations were below $1\,\mathrm{\mu g\,m}^{-3}$, mixing of the plume with background aerosol cannot explain this increase. Rather, it is likely that WSOM formed in the plume, potentially contributing to the observed growth of newly formed particles. In the most aged plume (A3), WSOM and AMS total organic concentrations still reach 3.4 and $48.4\,\mathrm{\mu g\,m}^{-3}$, respectively, showing that SOA production largely compensated for plume dilution.

On both days, the O : C ratio and the relative contribution of WSOM to AMS total organic concentration increased as the plume aged, indicating a change in the functionality of the organic aerosol. Since the chemical measurements are mass based, the chemical composition data on 17 July in plume age A1 are most representative of the larger, primary plume particles, which dominate the volume distribution (Fig. 3c). The primary plume particles are therefore characterized by low O : C ratios (< 0.001) and few water-soluble components (WSOM : Org ~ 0.002). At plume age A3, accumulation mode particles, which likely have grown out of the nucleation mode, are dominant in the volume distribution. Ratios of O : C and WSOM : Org at A3 are approximately 0.2 and 0.07, respectively, showing that the organic fraction of the small mode aerosol is more oxidized than that of the large mode. During A2, the volume is more evenly distributed over the primary and secondary plume particles. For this plume age, it is not obvious whether the increasing O : C ratio and the observed production of WSOM are mostly properties of the new, growing particles or a result of the aging of the primary particles,

or both. On 18 July (Fig. 7b), new particle formation was not observed and the volume distribution was at all times dominated by particles with diameters > 100 nm. An increase in O : C and WSOM : Org is observed, suggesting that a chemical transformation to more oxidized and more water-soluble compounds occurred in the primary plume particles.

Figure 8 shows a comparison of the FTIR spectra of plume particles sampled during ages A1 and A2 ("A1+A2") on 17 and 18 July, and aged particles sampled during A3 on 17 July, as well as the spectrum of particles directly emitted from the ship stack. For comparison, the spectra of laboratory samples of the oil used for smoke generation and the diesel used for fuel in the ship's engine are shown as well. The spectra all show absorbance at 3000–2800 cm^{-1}, which is indicative of alkane functional groups. The individual peaks at 2920 and 2850 cm^{-1} indicate the presence of methylene groups (Pavia et al., 2001). An increase in hydroxyl functional groups (3700–3100 cm^{-1}) can be observed in the spectrum of the ship stack compared to the laboratory spectrum of the ship diesel. Similarly, the spectrum of the smoke oil shows a higher peak in hydroxyl than the spectrum of the fresh smoke. These relative increases in hydroxyl functional groups are indicative of oxidization of the particles. In the aged particles on 17 July, an increase in hydroxyl and a decrease in alkane functional groups are evident, implying increased oxidation with increased aging. This increase in hydroxyl functional groups with the age of particles is consistent with the increase in O : C observed by the AMS.

The size-resolved AMS measurements of organic mass (Fig. 9) clearly show the larger plume mode in the size range 500–800 nm for both plume sampling events. The newly emerging particle mode at A2 and the grown particles at A3 are also clearly visible on 17 July (Fig. 9a). The organic marker m/z 57, which is associated with aliphatic organics (C$_4$H$_9^+$) and serves as a tracer for hydrocarbon-like organic aerosol (Zhang et al., 2005), is strongly related to the larger aerosol particles in the plume on both days, and does not appear in the smaller emerging mode. High-resolution AMS data show that C$_4$H$_9^+$ was indeed the dominant fragment in m/z 57 in the fresh plume. The marker m/z 44, dominated by acid-like oxygenates, was not found to contribute substantially

to any of the two modes. The organic marker m/z 43, however, is a component of both the larger and smaller mode.

High-resolution AMS data were examined to understand the contribution of m/z 43 to both modes. Two fragments govern m/z 43: $C_3H_7^+$ from alkyl groups and $C_2H_3O^+$ from non-acid oxygenates (Ng et al., 2011). In ambient aerosols, the organic marker m/z 43 is expected to be dominated by non-acid oxygenates (Ng et al., 2010). $C_2H_3O^+$ has also been found to be a major component in laboratory generated SOA from primary anthropogenic sources (Heringa et al., 2012). When examining the temporal behavior of the fragments $C_2H_3O^+$ and $C_3H_7^+$ together with the integrated aerosol volumes for the small (particle diameter < 100 nm) and the large (particle diameter > 100 nm) mode (Fig. 10), it is obvious that on both days, $C_3H_7^+$ traces the large mode volume. $C_2H_3O^+$, in contrast, traces the small particle volume, in particular on 17 July, where the formation and growth of particles gives rise to the small mode. The correlations between $C_3H_7^+$ and the large mode are significant on both days, whereas $C_2H_3O^+$ only shows a significant correlation with the small mode volume on 17 July (Table 3). This indicates that the small mode comprises more oxygenated compounds than the large mode.

4 Discussion: water-uptake and chemical composition

4.1 CCN activity

On 17 July, both the newly-formed particles (initially CCN inactive; small and non-hygroscopic) and the primary plume particles (initially CCN active; large and non-hygroscopic) contributed to CCN concentrations at medium ($0.24 < S < 0.26$ %) and high ($0.87 < S < 0.88$ %) supersaturations. Growth of newly-formed particles enriched with organics into CCN-relevant size ranges and chemical transformations were drivers for increasing CCN concentrations (Sect. 3.3). Larger, mostly organic primary plume particles also caused an increase in CCN concentrations on 18 July. Chemical

transformations and the condensation of hydrophilic organics within the given aging time can explain the observed CCN activity at medium S on both days: very short aging times (no more than a few hours) to convert hydrophobic particles into CCN have been observed in laboratory experiments (Tritscher et al., 2011), and suggested for atmospheric particles, particularly in daytime conditions with photochemical production of secondary aerosol mass (Wang et al., 2010). The CCN activity at high supersaturations can be explained without invoking organic transformation: even trace amounts of hygroscopic material (e.g., sulfate) deposited at the surface of the particle can lead to activation and droplet growth. Such inorganic trace components would be hard to detect by the mass-sensitive online chemical measurement methods and would contribute little to hygroscopic growth, which is sensitive to volume fractions of hygroscopic material. Similarly, insoluble, but wettable organic substances would result in little or no hygroscopic growth, but allow for activation as a CCN.

4.2 Hygroscopic growth factors

Contrary to CCN activity at high supersaturations, trace amounts of inorganic compounds cannot explain the increase in growth factors on 17 July: size-resolved chemical composition data indicate that inorganic mass fractions were very low at all particle sizes, and very hard to quantify for particle diameters < 100 nm, where the concentrations of many inorganic species were close to the detection limit.

The organic aerosol in the plume underwent an overall chemical transformation leading to higher O : C ratios, from < 0.001 in the fresh plume to values around 0.2 in the plume at age A3 (Fig. 7a). An increase in GF of 150 nm particles (most representative of primary plume particles) was observed over three scans (each an average over one up- and one down-scan of DMA 2): from 1.02 at 11:38 to 1.09 at 12:20 and 1.1 at 12:39 (92 % RH). Similarly, there was modest hygroscopic growth for 30 nm particles: GF = 1.05 at 12:12, and GF = 1.09 at 12:31 and 12:50. Based on previous work on ambient aerosols (Jimenez et al., 2009; Duplissy et al., 2011), no substantial hygroscopic growth is expected for O : C < 0.2. However, the measured O : C ratios and GFs

compare well with a chamber study on aging diesel exhaust, in which O : C ratios were observed to increase from 0.1–0.19 within < 2 h, while simultaneously, GFs increased from 1 to 1.1 (95 % RH, 100 nm dry particle diameter) (Tritscher et al., 2011).

Since the primary plume particles emitted from the R/V *Point Sur* were quite large (several hundred nm), the bulk chemical composition measurements cannot be assumed to be fully representative of the chemical composition of smaller particle sizes (30, 75 and 150 nm), for which the hygroscopic growth factors were measured. For the 30 nm dry particle size, the size-resolved chemical measurements are not very reliable due to the small amount of mass residing at that size. However, measurements of the organic concentrations at the center of the two modes of the plume (the primary mode at 500–800 nm and the emerging mode of ∼ 100 nm at plume age A3) were well above the detection limit and indicate that a more oxygenated form of organic aerosol was present in the growing small mode as compared to the large primary mode (Sect. 3.5). Therefore, assuming that the 30 nm particles are purely organic, the modest hygroscopic growth at 30 nm may be explained by the more oxygenated compounds, as indicated by the oxygenated ($C_2H_3O^+$) state of m/z 43 in the small particle mode, as opposed to the more hydrocarbon-like ($C_3H_7^+$) state of m/z 43 in the large particle mode. The growth factor increase at 150 nm may be due to growth of the emerging mode into the 150 nm size range, or due to condensation of the VOCs onto the preexisting primary plume particles.

On 18 July, the GF increase for 150 nm particles is much larger than on 17 July, and also harder to explain. The O : C and WSOM : Org increases are comparable to those of 17 July. The measured O : C values do not explain the range of GFs (up to 1.47). Based on the findings of Jimenez et al. (2009), for a purely organic particle, an O : C ratio of 0.55–0.6 is required to result in a GF of 1.5. There are no other obvious indicators of an increasingly more hydrophilic organic component on 18 July. However, in the absence of the newly emerging mode, mass concentrations below about 200 nm were very low. Bulk chemical measurements are therefore not representative of particles with a 150 nm dry size. Size-resolved AMS measurements at that size are close to the

detection limit and therefore less reliable. Additionally, there was no plume age A3 to compare to the intermediate plume age A2. We suggest the following explanations for the increasing GF on 18 July: (i) internal mixing with inorganic compounds, in particular sulfate. On 17 July, the 150 nm particles likely grew out of smaller particles through condensation of VOCs (assuming higher VOC levels on the sunny than on the foggy day), and may therefore contain higher organic mass fractions than those on 18 July. (ii) Aqueous-phase processing of organics towards more hygroscopic organic species, as has been documented before in the region (e.g., Crahan et al., 2004; Sorooshian et al., 2007). The expected higher O : C ratios resulting from aqueous-phase processing may not be reflected in the bulk measurement of O : C, for the reasons stated above. Filter samples show that two particulate species that are tracers for cloud processing the region (Crahan et al., 2004; Sorooshian et al., 2007) were observed in PM_{10} samples of the smoke on 18 July, but not on 17 July: oxalate ($236\,\mathrm{ng\,m^{-3}}$), and glyoxylate ($79\,\mathrm{ng\,m^{-3}}$). Oxalate is also associated with coarse crustal matter (e.g., Wang et al., 2012); however, its simultaneous detection with glyoxylate only on 18 July suggests that cloud processing was an important factor on that day. Another, more speculative explanation is that surface organic films may have prevented water uptake on 17 July and formed a kinetic barrier, which may have been "broken" by the higher RH on 18 July. However, the time scales over which such a barrier would operate are not known (McFiggans et al., 2006).

5 Summary and conclusions

We have shown substantial differences in hygroscopic growth and CCN activity of organic particles emitted in the marine atmosphere under different meteorological conditions. In sunny conditions, new particle formation occurred and originated from VOCs emitted together with or evaporated from larger primary plume particles. The organic fragment m/z 43 appeared both in the large plume particles and in the newly emerging mode, but with differing dominant fragments: $C_3H_7^+$ (alkyl groups) was dominant in

the large particle mode, $C_2H_3O^+$ (non-acid oxygenates) in the smaller mode, showing
that the newly-formed particles consisted of more oxygenated organic compounds. No
growth of particles from 10 to 100 nm was observed in the aged plume in foggy con-
ditions. Most likely, photo-oxidation of plume VOCs leading to new particle formation
was less efficient due to the reduced solar flux. Additionally, the fog droplets may have
acted as a sink for VOCs and small particles due to the large surface area they provide
for diffusive deposition.

Meteorological conditions have a profound impact on size distributions and CCN
yield of the plume particles. The majority of the initial plume particles did not act as
CCN. However, the newly-formed particles activated as CCN after growing into the ap-
propriate size ranges, in particularly great numbers ($> 4000\,cm^{-3}$) at high supersatura-
tions ($S = 0.8\,\%$). Newly-formed particles, comprised largely of SOA, can thus provide
high concentrations of CCN, as was found in other studies (Hennigan et al., 2012). In
the foggy conditions without new particle formation, the number concentration of CCN
produced by the plume was lower by an order of magnitude.

In sunny conditions, plume particles with a dry size of 30 nm showed limited hygro-
scopic growth (GF = 1.05–1.09 at RH = 92 %), while those with a dry size of 75 nm did
not grow at all. Particles with a dry diameter of 150 nm also showed little hygroscopic
growth (GF =1.02–1.1). The observed hygroscopic growth can be explained by mixing
with inorganic components, or by aging of the organic fraction, which was reflected in
increasing ratios of O : C and WSOM : Org. While the increase in O : C from < 0.001 to
~ 0.2 is below what is observed to influence GFs in ambient organic aerosols (Jimenez
et al., 2009), both the range of O : C and that of GFs are consistent with a cham-
ber study of aging primary organic aerosol (Tritscher et al., 2011). This shows that
the aging time to transform a pure hydrocarbon-like aerosol of the kind emitted in this
experiment to a hygroscopic organic aerosol of the kind found in many ambient mea-
surements is longer than the 1–4 h that were available in this study in clean marine
conditions. The aging time for the same particles to act as CCN, in contrast, is much
shorter (< 1 h). On the foggy day, GFs of 150 nm particles increased to up to 1.47 as

Title Page

Abstract | Introduction

Conclusions | References

Tables | Figures

|◀ | ▶|

◀ | ▶

Back | Close

Full Screen / Esc

Printer-friendly Version

Interactive Discussion

the plume aged. A different degree of internal mixing with hygroscopic inorganic compounds and/or aqueous-phase processing are suggested as possible explanations for this behavior.

References

Aiken, A. C., DeCarlo, P. F., and Jimenez, J. L.: Elemental analysis of organic species with electron ionization high-resolution mass spectrometry, Anal. Chem., 79, 8350–8358, doi:10.1021/ac071150w, 2007.

Allan, J. D., Topping, D. O., Good, N., Irwin, M., Flynn, M., Williams, P. I., Coe, H., Baker, A. R., Martino, M., Niedermeier, N., Wiedensohler, A., Lehmann, S., Müller, K., Herrmann, H., and McFiggans, G.: Composition and properties of atmospheric particles in the eastern Atlantic and impacts on gas phase uptake rates, Atmos. Chem. Phys., 9, 9299–9314, doi:10.5194/acp-9-9299-2009, 2009.

Bateman, A. P., Nizkorodov, S. A., Laskin, J., and Laskin, A.: Photolytic processing of secondary organic aerosols dissolved in cloud droplets, Phys. Chem. Chem. Phys., 13, 12199–12212, doi:10.1039/c1cp20526a, 2011.

Blando, J. D. and Turpin, B. J.: Secondary organic aerosol formation in cloud and fog droplets: a literature evaluation of plausibility, Atmos. Environ., 34, 1623–1632, doi:10.1016/S1352-2310(99)00392-1, 2000.

Burkart, J., Hitzenberger, R., Reischl, G., Bauer, H., Leder, K., and Puxbaum, H.: Activation of "synthetic ambient" aerosols – Relation to chemical composition of particles < 100 nm, Atmos. Environ., 54, 583–591, doi:10.1016/j.atmosenv.2012.01.063, 2012.

Cavalli, F., Facchini, M. C., Decesari, S., Mircea, M., Emblico, L., Fuzzi, S., Ceburnis, D., Yoon, Y. J., O'Dowd, C. D., Putaud, J.-P., and Dell'Acqua, A.: Advances in characterization of size-resolved organic matter in marine aerosol over the North Atlantic, J. Geophys. Res., 109, D24215, doi:10.1029/2004JD005137, 2004.

Coggon, M. M., Sorooshian, A., Wang, Z., Metcalf, A. R., Frossard, A. A., Lin, J. J., Craven, J. S., Nenes, A., Jonsson, H. H., Russell, L. M., Flagan, R. C., and Seinfeld, J. H.: Ship impacts on the marine atmosphere: insights into the contribution of shipping emissions to the properties of marine aerosol and clouds, Atmos. Chem. Phys., 12, 8439–8458, doi:10.5194/acp-12-8439-2012, 2012.

Crahan, K. K., Hegg, D., Covert, D. S., and Jonsson, H.: An exploration of aqueous oxalic acid production in the coastal marine atmosphere, Atmos. Environ., 38, 3757–3764, doi:10.1016/j.atmosenv.2004.04.009, 2004.

Dall'Osto, M., Ceburnis, D., Monahan, C., Worsnop, D. R., Bialek, J., Kulmala, M., Kurtén, T., Ehn, M., Wenger, J., Sodeau, J., Healy, R., and O'Dowd, C.: Nitrogenated and aliphatic organic vapors as possible drivers for marine secondary organic aerosol growth, J. Geophys. Res., 117, D12311, doi:10.1029/2012JD017522, 2012.

DeCarlo, P. F., Slowik, J. G., Worsnop, D. R., Davidovits, P., and Jimenez, J. L.: Particle morphology and density characterization by combined mobility and aerodynamic diameter measurements. Part 1: theory, Aerosol Sci. Technol., 38, 1180–1205, doi:10.1080/027868290903907, 2004.

DeCarlo, P. F., Kimmel, J. R., Trimborn, A., Northway, M. J., Jayne, J. T., Aiken, A. C., Gonin, M., Fuhrer, K., Horvath, T., Docherty, K. S., Worsnop, D. R., and Jimenez, J. L.: Field-deployable, high-resolution, time-of-flight aerosol mass spectrometer, Anal. Chem., 78, 8281–8289, doi:10.1021/ac061249n, 2006.

de Gouw, J. A., Middlebrook, A. M., Warneke, C., Ahmadov, R., Atlas, E. L., Bahreini, R., Blake, D. R., Brock, C. A., Brioude, J., Fahey, D. W., Fehsenfeld, F. C., Holloway, J. S., Le Henaff, M., Lueb, R. A., McKeen, S. A., Meagher, J. F., Murphy, D. M., Paris, C., Parrish, D. D., Perring, A. E., Pollack, I. B., Ravishankara, A. R., Robinson, A. L., Ryerson, T. B., Schwarz, J. P., Spackman, J. R., Srinivasan, A., and Watts, L. A.: Organic aerosol formation downwind from

Title Page

Abstract | Introduction

Conclusions | References

Tables | Figures

|◀ | ▶|

◀ | ▶

Back | Close

Full Screen / Esc

Printer-friendly Version

Interactive Discussion

the Deepwater Horizon oil spill, Science, 331, 1295–1299, doi:10.1126/science.1200320, 2011.

Dick, W. D., Saxena, P., and McMurry, P. H.: Estimation of water uptake by organic compounds in submicron aerosols measured during the southeastern aerosol and visibility study, J. Geophys. Res., 105, 1471–1479, doi:10.1029/1999JD901001, 2000.

Draxler, R. R. and Rolph, G. D.: HYSPLIT (HYbrid Single-Particle Lagrangian Integrated Trajectory) Model, access via NOAA ARL READY Website, available at: http://ready.arl.noaa.gov/HYSPLIT.php, last access: August 2012, NOAA Air Resources Laboratory, Silver Spring, MD, 2012.

Duplissy, J., DeCarlo, P. F., Dommen, J., Alfarra, M. R., Metzger, A., Barmpadimos, I., Prevot, A. S. H., Weingartner, E., Tritscher, T., Gysel, M., Aiken, A. C., Jimenez, J. L., Canagaratna, M. R., Worsnop, D. R., Collins, D. R., Tomlinson, J., and Baltensperger, U.: Relating hygroscopicity and composition of organic aerosol particulate matter, Atmos. Chem. Phys., 11, 1155–1165, doi:10.5194/acp-11-1155-2011, 2011.

Dusek, U., Frank, G. P., Massling, A., Zeromskiene, K., Iinuma, Y., Schmid, O., Helas, G., Hennig, T., Wiedensohler, A., and Andreae, M. O.: Water uptake by biomass burning aerosol at sub- and supersaturated conditions: closure studies and implications for the role of organics, Atmos. Chem. Phys., 11, 9519–9532, doi:10.5194/acp-11-9519-2011, 2011.

El Haddad, I., Yao Liu, Nieto-Gligorovski, L., Michaud, V., Temime-Roussel, B., Quivet, E., Marchand, N., Sellegri, K., and Monod, A.: In-cloud processes of methacrolein under simulated conditions – Part 2: Formation of secondary organic aerosol, Atmos. Chem. Phys., 9, 5107–5117, doi:10.5194/acp-9-5107-2009, 2009.

Ervens, B., Turpin, B. J., and Weber, R. J.: Secondary organic aerosol formation in cloud droplets and aqueous particles (aqSOA): a review of laboratory, field and model studies, Atmos. Chem. Phys., 11, 11069–11102, doi:10.5194/acp-11-11069-2011, 2011.

Eyring, V., Isaksen, I. S. A., Berntsen, T., Collins, W. J., Corbett, J. J., Endresen, O., Grainger, R., G., Moldanova, J., Schlager, H., and Stevenson, D. S.: Transport impacts on atmosphere and climate: shipping, Atmos. Environ., 44, 4735–4771, doi:10.1016/j.atmosenv.2009.04.059, 2009.

Facchini, M. C., Rinaldi, M., Decesari, S., Carbone, C., Finessi, E., Mircea, M., Fuzzi, S., Ceburnis, Flanagan, R., Nilsson, E. D., de Leeuw, G. D., Martino, M., Woeltjen, J., and O'Dowd, C.: Primary submicron marine aerosol dominated by insoluble organic colloids and aggregates, Geophys. Res. Lett., 35, L17814, doi:10.1029/2008GL034210, 2008a.

Title Page

Abstract | Introduction

Conclusions | References

Tables | Figures

◀ | ▶

◀ | ▶

Back | Close

Full Screen / Esc

Printer-friendly Version

Interactive Discussion

Facchini, M. C., Decesari, S., Rinaldi, M., Carbone, C., Finessi, E., Mircea, M., Fuzzi, S., Moretti, F., Tagliavini, E., Ceburnis, D., and O'Dowd, C.: Important source of marine secondary organic aerosol from biogenic amines, Environ. Sci. Technol., 42, 9116–9121, doi:10.1021/es8018385, 2008b.

Feingold, G., Walko, R. L., Stevens, B., and Cotton, W. R.: Simulations of marine stratocumulus using a new microphysical parameterization scheme, Atmos. Res., 47–48, 505–528, doi:10.1016/S0169-8095(98)00058-1, 1998.

Frossard, A. A. and Russell, L. M.: Removal of sea salt hydrate water from seawater-derived samples by dehydration, Environ. Sci. Tech., 46, 13326–13333, doi:10.1021/es3032083, 2012.

Furutani, H., Dall'osto, M., Roberts, G. C., and Prather, K. A.: Assessment of the relative importance of atmospheric aging on CCN activity derived from field observations, Atmos. Environ., 42, 3130–3142, doi:10.1016/j.atmosenv.2007.09.024, 2008.

Gantt, B. and Meskhidze, N.: The physical and chemical characteristics of marine primary organic aerosol: a review, Atmos. Chem. Phys., 13, 3979–3996, doi:10.5194/acp-13-3979-2013, 2013.

George, I. J., Vlasenko, A., Slowik, J. G., Broekhuizen, K., and Abbatt, J. P. D.: Heterogeneous oxidation of saturated organic aerosols by hydroxyl radicals: uptake kinetics, condensed-phase products, and particle size change, Atmos. Chem. Phys., 7, 4187–4201, doi:10.5194/acp-7-4187-2007, 2007.

Gysel, M., McFiggans, G. B., and Coe, H.: Inversion of tandem differential mobility analyser (TDMA) measurements, J. Aerosol Sci., 40, 134–151, doi:10.1016/j.jaerosci.2008.07.013, 2009.

Hawkins, L. N., Russell, L. M., Covert, D. S., Quinn, P. K., and Bates, T. S.: Carboxylic acids, sulfates and organosulfates in processed continental organic aerosol over the southern Pacific Ocean during VOCALS-Rex 2008, J. Geophys. Res., 115, D13201, doi:10.1029/2009JD013276, 2010.

Hegg, D. A.: The importance of liquid phase oxidation of SO_2 in the atmosphere, J. Geophys. Res., 90, 3773–3779, doi:10.1029/JD090iD02p03773, 1985.

Hegg, D. A., Covert, D. S., Jonsson, H. H., and Woods, R. K.: The contribution of anthropogenic aerosols to aerosol light-scattering and CCN activity in the California coastal zone, Atmos. Chem. Phys., 10, 7341–7351, doi:10.5194/acp-10-7341-2010, 2010.

Emitted organic plume

A. Wonaschütz et al.

Title Page

Abstract | Introduction

Conclusions | References

Tables | Figures

|◄ | ►|

◄ | ►

Back | Close

Full Screen / Esc

Printer-friendly Version

Interactive Discussion

Hennigan, C. J., Westervelt, D. M., Riipinen, I., Engelhart, G. J., Lee, T., Collett, J. L., Pandis, S. N., Adams, P. J., and Robinson, A. L.: New particle formation and growth in biomass burning plumes: An important source of cloud condensation nuclei, Geophys. Res. Lett., 39, L09805, doi:10.1029/2012GL050930, 2012.

Heringa, M. F., DeCarlo, P. F., Chirico, R., Tritscher, T., Clairotte, M., Mohr, C., Crippa, M., Slowik, J. G., Pfaffenberger, L., Dommen, J., Weingartner, E., Prévôt, A. S. H., and Baltensperger, U.: A new method to discriminate secondary organic aerosols from different sources using high-resolution aerosol mass spectra, Atmos. Chem. Phys., 12, 2189–2203, doi:10.5194/acp-12-2189-2012, 2012.

Hersey, S. P., Sorooshian, A., Murphy, S. M., Flagan, R. C., and Seinfeld, J. H.: Aerosol hygroscopicity in the marine atmosphere: a closure study using high-time-resolution, multiple-RH DASH-SP and size-resolved C-ToF-AMS data, Atmos. Chem. Phys., 9, 2543–2554, doi:10.5194/acp-9-2543-2009, 2009.

Hersey, S. P., Craven, J. S., Metcalf, A. R., Lin, J., Lathem, T., Suski, K., Cahill, J., Duong, H., Sorooshian, A., Jonsson, H. H., Nenes, A., Prather, K. A., Flagan, R. C., and Seinfeld, J. H.: Composition and hygroscopicity of the Los Angeles Aerosol: CalNex, J. Geophys. Res., 118, 3016–3036, doi:10.1002/jgrd.50307, 2013.

Hoppel, W. A., Frick, G. M., and Fitzgerald, J. W.: Deducing droplet concentration and supersaturation in marine boundary layer clouds from surface aerosol measurements, J. Geophys. Res., 101, 26553–26565, doi:10.1029/96JD02243, 1996.

Jimenez, J. L., Canagaratna, M. R., Donahue, N. M., Prevot, A. S. H., Zhang, Q., Kroll, J. H., DeCarlo, P. F., Allan, J. D., Coe, H., Ng, N. L., Aiken, A. C., Docherty, K. S., Ulbrich, I. M., Grieshop, A. P., Robinson, A. L., Duplissy, J., Smith, J. D., Wilson, K. R., Lanz, V. A., Hueglin, C., Sun, Y. L., Tian, J., Laaksonen, A., Raatikainen, T., Rautiainen, J., Vaattovaara, P., Ehn, M., Kulmala, M., Tomlinson, J. M., Collins, D. R., Cubison, M. J., Dunlea, E. J., Huffman, J. A., Onasch, T. B., Alfarra, M. R., Williams, P. I., Bower, K., Kondo, Y., Schneider, J., Drewnick, F., Borrmann, S., Weimer, S., Demerjian, K., Salcedo, D., Cottrell, L., Griffin, R., Takami, A., Miyoshi, T., Hatakeyama, S., Shimono, A., Sun, J. Y., Zhang, Y. M., Dzepina, K., Kimmel, J.R., Sueper, D., Jayne, J. T., Herndon, S. C., Trimborn, A. M., Williams, L. R., Wood, E. C., Middlebrook, A. M., Kolb, C. E., Baltensperger, U., and Worsnop, D. R.: Evolution of organic aerosols in the atmosphere, Science, 326, 1525–1529, doi:10.1126/science.1180353, 2009.

Title Page

Abstract | Introduction

Conclusions | References

Tables | Figures

|◄ | ►|

◄ | ►

Back | Close

Full Screen / Esc

Printer-friendly Version

Interactive Discussion

Khlystov, A., Stanier, C., and Pandis, S. N.: An algorithm for combining electrical mobility and aerodynamic size distributions data when measuring ambient aerosol, Aerosol Sci. Technol., 38, 229–238, doi:10.1080/02786820390229543, 2004.

Leck, C. and Bigg, E. K.: Source and evolution of the marine aerosol – a new perspective, Geophys. Res. Lett., 32, L19803, doi:10.1029/2005GL023651, 2005.

Massling, A., Leinert, S., Wiedensohler, A., and Covert, D.: Hygroscopic growth of sub-micrometer and one-micrometer aerosol particles measured during ACE-Asia, Atmos. Chem. Phys., 7, 3249–3259, doi:10.5194/acp-7-3249-2007, 2007.

Massoli, P., Lambe, A. T., Ahern, A. T., Williams, L. R., Ehn, M., Mikkilä, J., Canagaratna, M. R., Brune, W. H., Onasch, T. B., Jayne, J. T., Petäjä, T., Kulmala, M., Laaksonen, A., Kolb, C. E., Davidovits, P., and Worsnop, D. R.: Relationship between aerosol oxidation level and hygroscopic properies of laboratory generated secondary organic aerosol (SOA) particles, Geophys. Res. Lett., 37, L24801, doi:10.1029/2010GL045258, 2010.

McFiggans, G., Artaxo, P., Baltensperger, U., Coe, H., Facchini, M. C., Feingold, G., Fuzzi, S., Gysel, M., Laaksonen, A., Lohmann, U., Mentel, T. F., Murphy, D. M., O'Dowd, C. D., Snider, J. R., and Weingartner, E.: The effect of physical and chemical aerosol properties on warm cloud droplet activation, Atmos. Chem. Phys., 6, 2593–2649, doi:10.5194/acp-6-2593-2006, 2006.

Meskhidze, N. and Nenes, A.: Phytoplankton and cloudiness in the Southern Ocean, Science, 314, 1419, doi:10.1126/science.1131779, 2006.

Metcalf, A. R.; Craven, J. S., Ensberg, J. J., Brioude, J., Angevine, W., Sorooshian, A., Duong, H. T., Jonsson, H. H., Flagan, R. C., and Seinfeld, J. H.: Black carbon aerosol over the Los Angeles Basin during CalNex, J. Geophys. Res., 117, D00V13, doi:10.1029/2011JD017255, 2012.

Meyer, N. K., Duplissy, J., Gysel, M., Metzger, A., Dommen, J., Weingartner, E., Alfarra, M. R., Prevot, A. S. H., Fletcher, C., Good, N., McFiggans, G., Jonsson, Å. M., Hallquist, M., Baltensperger, U., and Ristovski, Z. D.: Analysis of the hygroscopic and volatile properties of ammonium sulphate seeded and unseeded SOA particles, Atmos. Chem. Phys., 9, 721–732, doi:10.5194/acp-9-721-2009, 2009.

Middlebrook, A. M., Murphy, D. M., and Thomson, D. S.: Observations of organic material in individual marine particles at Cape Grim during the First Aerosol Characterization Experiment (ACE 1), J. Geophys. Res., 103, 16,475–16,483, doi:10.1029/97JD03719, 1998.

Mochida, M., Nishita-Hara, C., Furutani, H., Miyazaki, Y., Jung, J., Kawamura, K., and Ue-matsu, M.: Hygroscopicity and cloud condensation nucleus activity of marine particles over the western North Pacific, J. Geophys. Res., 116, D06204, doi:10.1029/2010JD014759, 2011.

Moore, R. H., Raatikainen, T., Langridge, J. M., Bahreini, R., Brock, C. A., Holloway, J. S., Lack, D. A., Middlebrook, A. M., Perring, A. E., Schwarz, J. P., Spackman, J. R., and Nenes, A.: CCN spectra, hygroscopicity, and droplet activation kinetics of secondary organic aerosol resulting from the 2010 Deepwater Horizon oil spill, Environ. Sci. Technol., 46, 3093–3100, doi:10.1021/es203362w, 2012.

Murphy, S. M., Agrawal, H., Sorooshian, A., Padro, L. T., Gates, H., Hersey, S., Welch, W. A., Jung, H., Miller, J. W., Cocker, D. R., Nenes, A., Jonsson, H. H., Flagan, R. C., and Seinfeld, J. H.: Comprehensive simultaneous shipboard and airborne characterization of exhaust from a modern container ship at sea, Environ. Sci. Technol., 43, 4626–4640, doi:10.1021/es802413j, 2009.

Ng, N. L., Canagaratna, M. R., Zhang, Q., Jimenez, J. L., Tian, J., Ulbrich, I. M., Kroll, J. H., Docherty, K. S., Chhabra, P. S., Bahreini, R., Murphy, S. M., Seinfeld, J. H., Hildebrandt, L., Donahue, N. M., DeCarlo, P. F., Lanz, V. A., Prévôt, A. S. H., Dinar, E., Rudich, Y., and Worsnop, D. R.: Organic aerosol components observed in Northern Hemispheric datasets from Aerosol Mass Spectrometry, Atmos. Chem. Phys., 10, 4625–4641, doi:10.5194/acp-10-4625-2010, 2010.

Ng, N. L., Canagaratna, M. R., Jimenez, J. L., Chhabra, P. S., Seinfeld, J. H., and Worsnop, D. R.: Changes in organic aerosol composition with aging inferred from aerosol mass spectra, Atmos. Chem. Phys., 11, 6465–6474, doi:10.5194/acp-11-6465-2011, 2011.

O'Dowd, C. D., Maria Cristina Facchini, M. C., Cavalli, F., Ceburnis, D., Mircea, M., Decesari, S., Fuzzi, S., Yoon, Y. J., and Putaud, J.-P.: Biogenically driven organic contribution to marine aerosol, Nature 431, 676–680, doi:10.1038/nature02959, 2004.

O'Dowd, C. D. and de Leeuw, G.: Marine aerosol production: a review of the current knowledge, Phil. Trans. R. Soc. A, 365, 1753–1774, doi:10.1098/rsta.2007.2043, 2007.

Ovadnevaite, J., Ceburnis, D., Martucci, G., Bialek, J., Monahan, C., Rinaldi, M., Facchini, M. C., Berresheim, H., Worsnop, D. R., and O'Dowd, C.: Primary marine organic aerosol: a dichotomy of low hygroscopicity and high CCN activity, Geophys. Res. Lett., 38, L21806, doi:10.1029/2011GL048869, 2011a.

Emitted organic plume

A. Wonaschütz et al.

Title Page

Abstract | Introduction

Conclusions | References

Tables | Figures

◄◄ | ►►

◄ | ►

Back | Close

Full Screen / Esc

Printer-friendly Version

Interactive Discussion

Ovadnevaite, J., O'Dowd, C., Dall'Osto, M., Ceburnis, D., Worsnop, D. R., and Berresheim, H.: Detecting high contributions of primary marine organic matter to marine aerosol: a case study, Geophys. Res. Lett., 38, L02807, doi:10.1029/2010GL046083, 2011b.

Pavia, D. L., Lapman, G. M., and Kriz, G. S.: Introduction to Spectroscopy, 3rd Edn., Brooks/Cole, 2001.

Petters, M. D. and Kreidenweis, S. M.: A single parameter representation of hygroscopic growth and cloud condensation nucleus activity, Atmos. Chem. Phys., 7, 1961–1971, doi:10.5194/acp-7-1961-2007, 2007.

Petters, M. D., Carrico, C. M., Kreidenweis, S. M., Prenni, A. J., DeMott, P. J., Collett, J. L., and Moosmuller, H.: cloud condensation nucleation activity of biomass burning aerosol, J. Geophys. Res., 114, D22205, doi:10.1029/2009JD012353, 2009.

Roberts, G. C. and Nenes, A.: A continuous-flow streamwise thermal-gradient CCN chamber for atmospheric measurements, Aerosol Sci. Technol., 39, 206–221, doi:10.1080/027868290913988, 2005.

Roberts, G. C., Artaxo, P., Zhou, J. C., Swietlicki, E., and Andreae, M. O.: Sensitivity of CCN spectra on chemical and physical properties of aerosol: a case study from the Amazon basin, J. Geophys. Res., 107, D20, doi:10.1029/2001JD000583, 2002.

Robinson, A. L., Donahue, N. M., Shrivastava, M. K., Weitkamp, E. A., Sage, A. M., Grieshop, A. P., Lane, T. E., Pierce, J. R., and Pandis, S. N.: Rethinking organic aerosols: semivolatile emissions and photochemical aging, Science, 315, doi:10.1126/science.1133061, 2007.

Russell, L. M., Takahama, S. Liu, S., Hawkins, L. N., Covert, D. S., Quinn, P. K., and Bates, T. S.: Oxygenated fraction and mass of organic aerosol from direct emission and atmospheric processing measured on the R/V Ronald Brown during TEXAQS/GoMACCS 2006, J. Geophys. Res., 114, doi:10.1029/2008jd011275, 2009.

Russell, L. M., Hawkins, L. N., Frossard, A. A., Quinn, P. K., and Bates, T. S.: Carbohydrate-like composition of submicron atmospheric particles and their production from ocean bubble bursting, P. Natl. Acad. Sci. USA, 107, 15, 6652–6657, doi:10.1073/pnas.0908905107, 2010.

Russell, L. M., Sorooshian, A., Seinfeld, J. H., Albrecht, B. A., Nenes, A., Ahlm, L., Chen, Y. C., Coggon, M., Craven, J. S., Flagan, R. C., Frossard, A. A., Jonsson, H., Jung, E., Lin, J. J., Metcalf, A. R., Modini, R., Mülmenstädt, J., Roberts, G. C., Shingler, T., Song, S., Wang, Z., and Wonaschütz, A.: Eastern Pacific Emitted Aerosol Cloud Experiment (E-PEACE), B. Am. Meteorol. Soc., 111, doi:10.1175/BAMS-D-12-00015, in press, 2013.

Title Page

Abstract | Introduction

Conclusions | References

Tables | Figures

|◄ | ►|

◄ | ►

Back | Close

Full Screen / Esc

Printer-friendly Version

Interactive Discussion

Saxena, P., Hildemann, L., McMurry, P. H., and Seinfeld, J. H.: Organics alter hygroscopic behavior of atmospheric particles, J. Geophys. Res., 100, D9, doi:10.1029/95JD01835, 1995.

Shingler, T., Dey, S., Sorooshian, A., Brechtel, F. J., Wang, Z., Metcalf, A., Coggon, M., Mülmenstädt, J., Russell, L. M., Jonsson, H. H., and Seinfeld, J. H.: Characterization and airborne deployment of a new counterflow virtual impactor inlet, Atmos. Meas. Tech. Discuss., 5, 1515–1541, doi:10.5194/amtd-5-1515-2012, 2012.

Sorooshian, A., Lu, M.-L., Brechtel, F. J., Jonsson, H., Feingold, G., Flagan, R. C., and Seinfeld, J. H., On the source of organic acid aerosol layers above clouds, Environ. Sci. Technol., 41, 4647–4654, doi:10.1021/es0630442, 2007.

Sorooshian, A., Padro, L. T., Nenes, A., Feingold, G., McComiskey, A., Hersey, S. P., Gates, H., Jonsson, H. H., Miller, S. D., Stephens, G. L., Flagan, R. C., and Seinfeld, J. H.: On the link between ocean biota emissions, aerosol, and maritime clouds: Airborne, ground, and satellite measurements off the coast of California, Global Biogeochem. Cy., 23, GB4007, doi:10.1029/2009GB003464, 2009.

Sorooshian, A., Murphy, S. M., Hersey, S., Bahreini, R., Jonsson, H., Flagan, R. C., and Seinfeld, J. H.: Constraining the contribution of organic acids and AMS m/z 44 to the organic aerosol budget: on the importance of meteorology, aerosol hygroscopicity, and region, Geophys. Res. Lett., 37, L21807, doi:10.1029/2010GL044951, 2010.

Sorooshian, A., Csavina, J., Shingler, T., Dey, S., Brechtel, F., Sáez, E., and Betterton, E. A.: Hygroscopic and chemical properties of aerosols collected near a copper smelter: implications for public and environmental health, Environ. Sci. Technol., 46, 9473–9480, doi:10.1021/es302275k, 2012.

Stolzenburg, M.: An Ultra-Fine Aerosol Size Distribution Measuring System, Ph.D. Thesis, University of Minnesota, Minneapolis, 1988.

Sullivan, A. P., Peltier, R. E., Brock, C. A., de Gouw, J. A, Holloway, J. S., Warneke, C., Wollny, A. G., and Weber, R. J.: Airborne measurements of carbonaceous aerosol soluble in water over northeastern united states: method development and an investigation into water-soluble organic carbon sources, J. Geophys. Res., 111, D23S46, doi:10.1029/2006jd007072, 2006.

Swietlicki, E., Hansson, H.-C., Hämeri, K., Svenningsson, B., Massling, A., McFiggans, G., McMurry, P. H., Petäja, T., Tunved, P., Gysel, M., Topping, D., Weingartner, E., Baltensperger, U., Rissler, J., Wiedensohler, A., and Kulmala, M.: Hygroscopic properties of submicrometer

Title Page

Abstract | Introduction

Conclusions | References

Tables | Figures

|◄ | ►|

◄ | ►

Back | Close

Full Screen / Esc

Printer-friendly Version

Interactive Discussion

atmospheric aerosol particles measured with H-TDMA instruments in various environments – a review, Tellus B, 60, 432–469, doi:10.1111/j.1600-0889.2008.00350.x, 2008.

Takahama, S., Johnson, A., and Russell, L. M.: Quantification of carboxylic and carbonyl functional groups in organic aerosol infrared absorbance spectra, Aerosol Sci. Technol., 47, 310–325, doi:10.1080/02786826.2012.752065, 2012.

Thouron, O., Brenguier, J.-L., and Burnet, F.: Supersaturation calculation in large eddy simulation models for prediction of the droplet number concentration, Geosci. Model Dev., 5, 761–772, doi:10.5194/gmd-5-761-2012, 2012.

Tritscher, T., Juranyi, Z., Martin, M., Chirico, R., Gysel, M., Heringa, M. F., deCarlo, P. F., Sierau, B., Prevot, A. S. H., Weingartner, E., and Baltensperger, U.: Changes of hygroscopicity and morphology during ageing of diesel soot, Environ. Res. Lett., 6, 034026, doi:10.1088/1748-9326/6/3/034026, 2011.

Turpin, B. J. and Lim, H.-J: Species contributions to $PM_{2.5}$ mass concentrations: revisiting common assumptions for estimating organic mass, Aerosol Sci. Technol., 35, 1, doi:10.1080/02786820152051454, 2001.

Wang, J., Cubison, M. J., Aiken, A. C., Jimenez, J. L., and Collins, D. R.: The importance of aerosol mixing state and size-resolved composition on CCN concentration and the variation of the importance with atmospheric aging of aerosols, Atmos. Chem. Phys., 10, 7267–7283, doi:10.5194/acp-10-7267-2010, 2010.

Wang, G., Kawamura, K., Cheng, C., Li, J., Cao, J., Zhang, R., Zhang, T., Liu, S., and Zhao, Z.: Molecular distribution and stable carbon isotopic composition of dicarboxylic acids, ketocarboxylic acids, and α-dicarbonyls in size-resolved atmospheric particles from Xi'an City, China, Environ. Sci. Technol., 46, 4783–4791, doi:10.1021/es204322c, 2012.

Wex, H., Stratmann, F., Hennig, T., Hartmann, S., Niedermeier, D., Nilsson, E., Ocskay, R., Rose, D., Salma, I. and Ziese, M.: Connecting hygroscopic growth at high humidities to cloud activation for different particle types, Environ. Res. Lett., 3, 035004 doi:10.1088/1748-9326/3/3/035004, 2008.

Wex, H., Petters, M. D., Carrico, C. M., Hallbauer, E., Massling, A., McMeeking, G. R., Poulain, L., Wu, Z., Kreidenweis, S. M., and Stratmann, F.: Towards closing the gap between hygroscopic growth and activation for secondary organic aerosol: Part 1 – Evidence from measurements, Atmos. Chem. Phys., 9, 3987–3997, doi:10.5194/acp-9-3987-2009, 2009.

Wonaschütz, A., Hersey, S. P., Sorooshian, A., Craven, J. S., Metcalf, A. R., Flagan, R. C., and Seinfeld, J. H.: Impact of a large wildfire on water-soluble organic aerosol in a major urban

Title Page

Abstract | Introduction

Conclusions | References

Tables | Figures

|◄ | ►|

◄ | ►

Back | Close

Full Screen / Esc

Printer-friendly Version

Interactive Discussion

area: the 2009 Station Fire in Los Angeles County, Atmos. Chem. Phys., 11, 8257–8270, doi:10.5194/acp-11-8257-2011, 2011.

Zhang, Q., Alfarra, M. R., Worsnop, D. R., Allan, J. D., Doe, H., Canagaratna, M., and Jimenez, J. L.: Deconvolution and quantification of hydrocarbon-like and oxygenated organic aerosols based on aerosol mass spectrometry, Environ. Sci. Technol., 39, 4938–4952, doi:10.1021/es048568l, 2005.

Title Page

Abstract | Introduction

Conclusions | References

Tables | Figures

◄ | ►

◄ | ►

Back | Close

Full Screen / Esc

Printer-friendly Version

Interactive Discussion

Table 1. Instruments on the R/V *Point Sur*.

Measurement	Instrument	Size range	Time resolution
Particle size distribution	APS	0.5–20 µm	2 min
	OPS	0.3–50 µm	2 min
	SEMS	10–946 nm	5 min
Number concentration	CPC	> 10 nm	1 s
Water uptake	CCN counter		9 s
	HTDMA (hygroscopic growth)	30, 75, 150, 300 nm	5 min
Chemical composition	AMS	< 1 µm	4 min
	PILS–TOC (water-soluble organic carbon)	< 1 µm	6 min
	SP2 (black carbon)	80–300 nm	10 s
	Filters scanned with FTIR spectroscopy	< 1 µm	20 min–4 h

Table 2. Hygroscopic growth factors (150 nm dry diameter) averaged over the two meteorological regimes. For the bold values, the difference of the means between Regime 1 and Regime 2 is statistically significant (95 % confidence level). "σ" denotes standard deviations.

150 nm	Regime 1		Regime 2	
RH	mean	σ	mean	σ
40 %	**1.06**	**0.03**	**1.04**	**0.03**
70 %	**1.24**	**0.04**	**1.21**	**0.03**
85 %	1.44	0.05	1.44	0.05
92 %	1.66	0.12	1.60	0.10

Table 3. Correlations (a = intercept, b = slope, n = number of samples) between the fragments $C_2H_3O^+$ and $C_3H_7^+$ and particle volume for the large and the small mode. Bold: correlation is statistically significant at the 99 % level. $C_3H_7^+$ correlates with the large mode on both days, $C_2H_3O^+$ correlates with the small mode on 17 July.

day	Mode	$C_3H_7^+$				$C_2H_3O^+$			
		a	b	r^2	n	a	b	r^2	n
17 Jul	volume > 100 nm	**−0.459**	**0.009**	**0.77**	**24**	0.270	0.001	0.16	22
	volume < 100 nm	2.881	−0.016	0.10	24	**0.247**	**0.006**	**0.39**	**22**
18 Jul	volume > 100 nm	**1.525**	**0.003**	**0.86**	**42**	0.247	1.418	0.01	41
	volume < 100 nm	3.765	0.859	0.03	42	0.275	−0.003	0.00	41
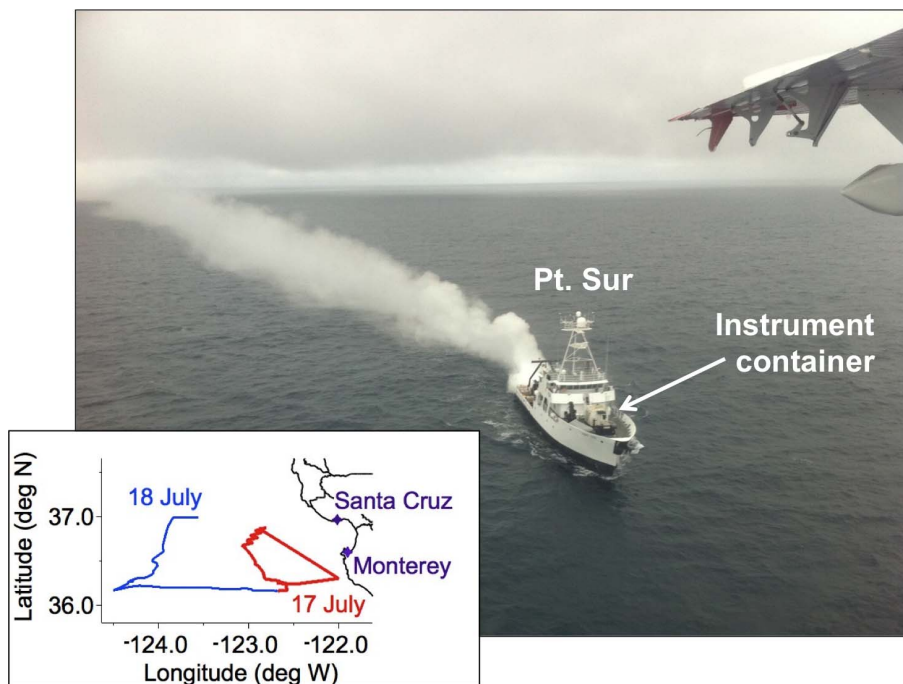
Fig. 1. Smoke generation on the R/V *Point Sur* (photo taken from CIRPAS Twin Otter). Insert: General area of the E-PEACE field campaign off the coast of California. The ship's track is shown for the days that are the focus of this study.
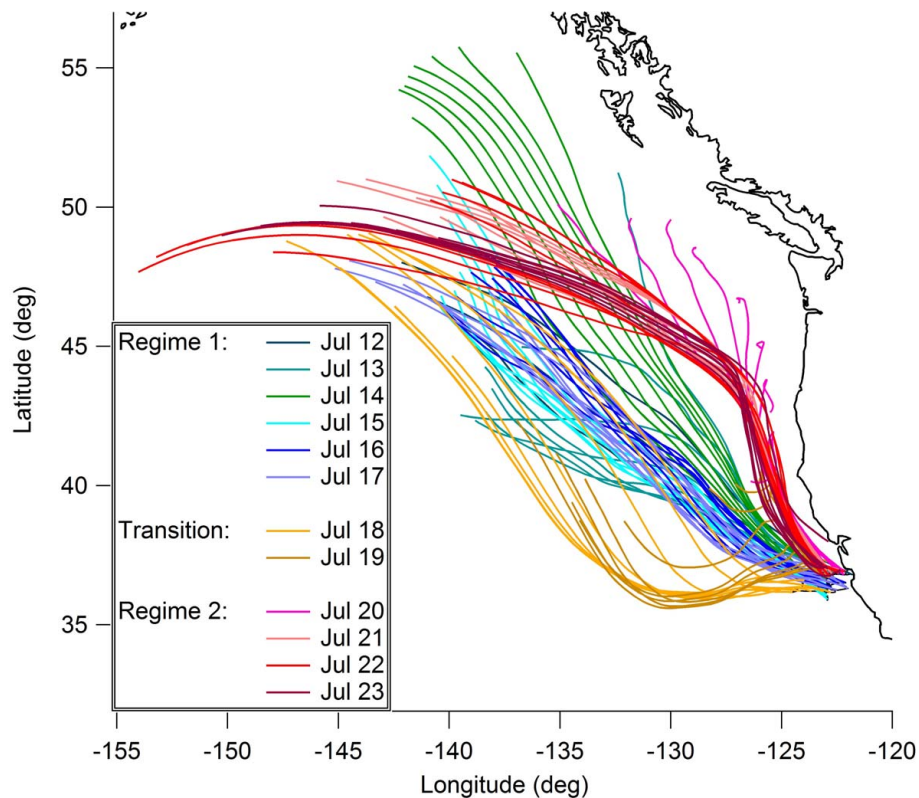
Fig. 2. Three-day HYSPLIT back-trajectories (every three hours, ending altitude: 50 m) show air mass origins during the cruise. Three distinct groups of trajectories governed by synoptic conditions are apparent: back-trajectories pertaining to Regime 1 (blue–green), Transition (orange), and Regime 2 (red).
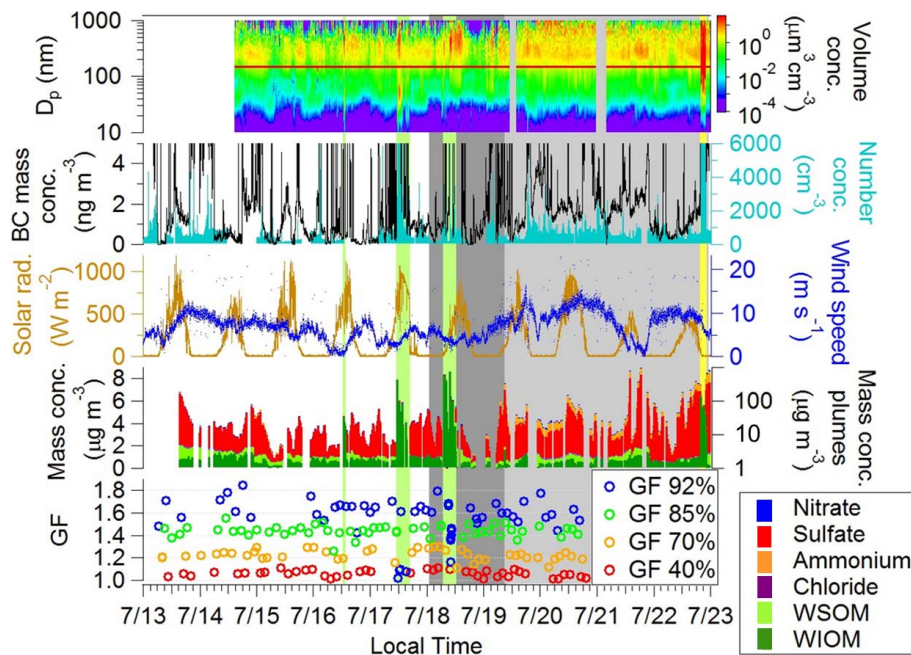
Fig. 3. Sub-µm volume distributions (DMA), total number concentrations $< 6000\,\mathrm{cm}^{-3}$ (CPC), black carbon concentrations $< 5\,\mathrm{ng\,m}^{-3}$ (SP2), chemical composition (AMS and PILS) and hygroscopic growth factors (HTDMA) for a dry particle size of 150 nm (indicated in the volume distributions (top panel) by the red line) and four different RHs, as a function of time over the entire research cruise. Green shading: plume; yellow shading: ship stack exhaust; no shading: Regime 1; dark gray shading: Transition; light gray shading: Regime 2. Mass concentrations for AMS and PILS in green or yellow shading (plumes) pertain to the right y-axis. Refer to Sect. 3.1 for more details.

Fig. 4. Ship trace during plume sampling by the R/V *Point Sur* on 17 July **(a)** and 18 July **(b)**. The plume location is identified by values of organic:sulfate > 5 (green markers). Black borders indicate high particle number concentrations. A1, A2 and A3 designate the three plume ages described in Sect. 2.6.
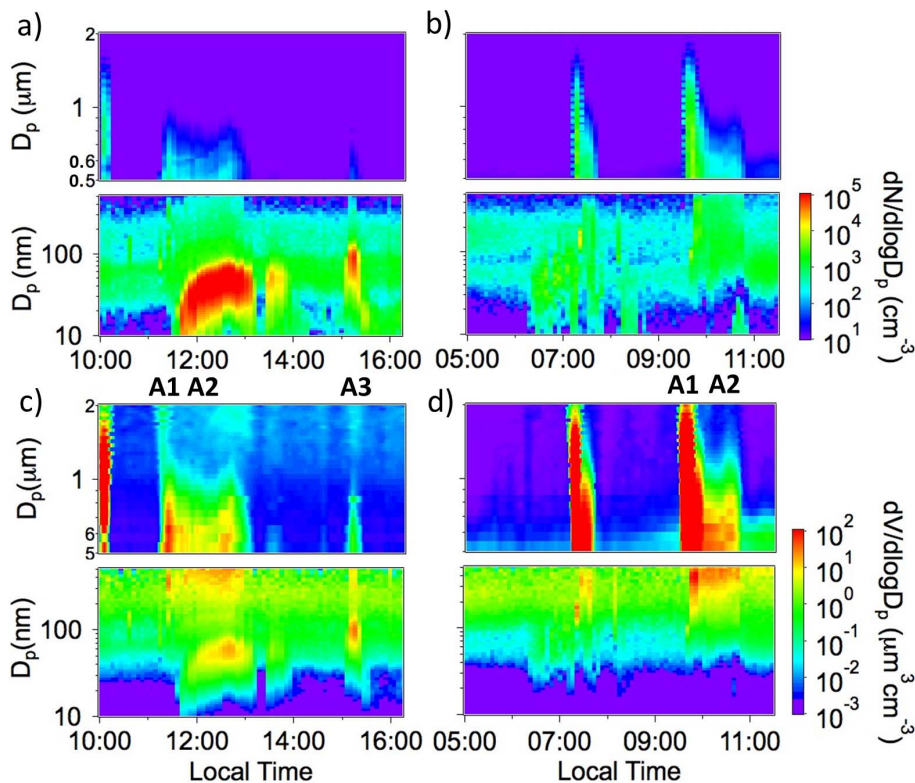
Fig. 5. Number **(a/b)** and volume **(c/d)** size distributions (DMA and APS/OPS) of the plume particles on 17 July **(a/c)** and 18 July **(b/d)**. A particle formation and growth event is observed on 17 July, which contributes substantial aerosol mass to the plume. Only large plume particles were detected on 18 July.
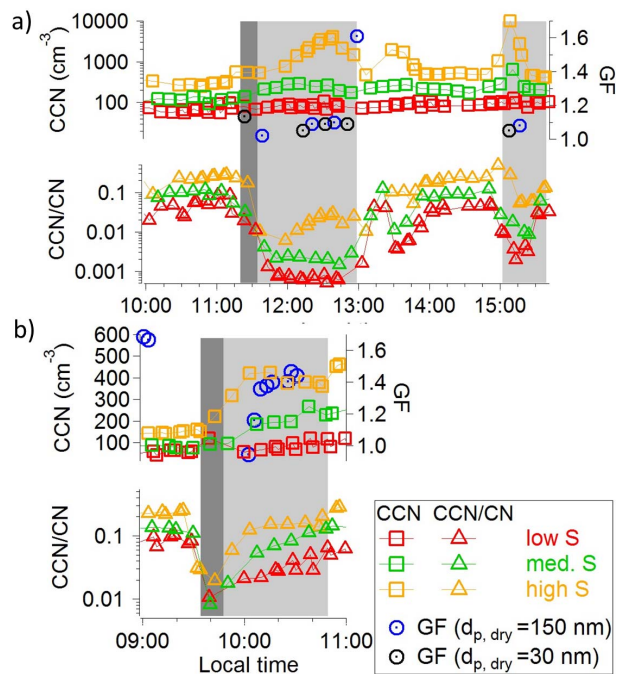
Fig. 6. Hygroscopic growth factors for 30 and 150 nm dry size at 92 % RH, and time series of CCN concentrations and activation ratios at three supersaturations: $0.07 < S < 0.08\%$ (red; low), $0.24 < S < 0.26\%$ (green; medium), and $0.87 < S < 0.88\%$ (yellow; high) for the plume sampling events on 17 July **(a)** and 18 July **(b)**. Dark gray shading designates plume age A1, light gray shading plume ages A2 and A3. Refer to Sects. 3.3 and 3.4 for more details.

Title Page

Abstract | Introduction

Conclusions | References

Tables | Figures

|◄ | ►|

◄ | ►

Back | Close

Full Screen / Esc

Printer-friendly Version

Interactive Discussion
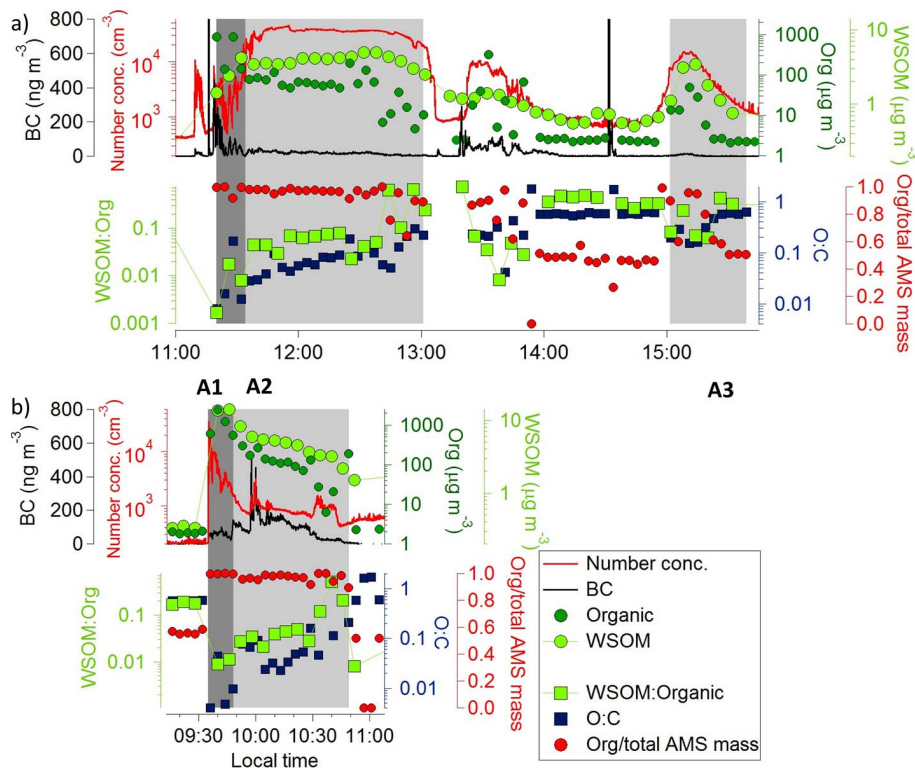
Fig. 7. Plume chemical composition measured by AMS for the three plume ages (A1, A2, A3) and marine background aerosol on 17 July **(a)** and 18 July **(b)**. As in Fig. 6, light gray shading designates plume ages A2 and A3, and dark gray shading represents the fresh plume (A1). The ratios O : C and WSOM : Org increase with plume age, an absolute increase of WSOM is observed on 17 July.
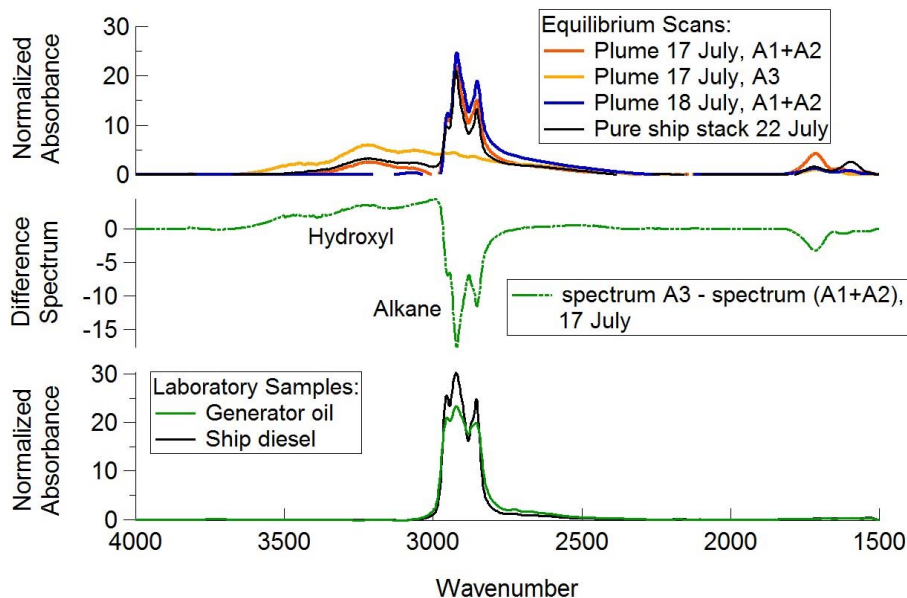
Fig. 8. FTIR spectra of the plume for a filter sample over ages A1 and A2 ("A1+A2"), and a sample for age A3 (upper panel) and their difference (middle panel). Spectra of the pure ship stack emissions (sampled on 22 July), as well as the smoke oil and the ship diesel fuel are shown for comparison (lower panel). Hydroxyl functional groups are detected in the aged smoke plume, but much less so in the fresh smoke and the laboratory samples.
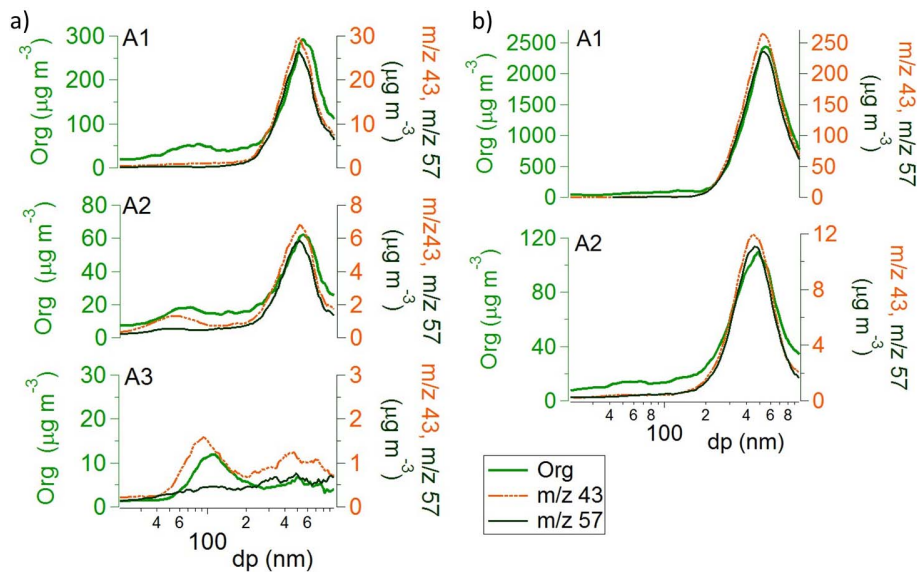
Fig. 9. Size resolved concentrations of AMS organic, and the organic markers m/z 57 and m/z 43 for 17 July **(a)** and 18 July **(b)**. The small particle mode is clearly visible on 17 July. The marker m/z 57 only appears in the large particle mode, the marker m/z 43 in both modes.

Printer-friendly Version

Interactive Discussion
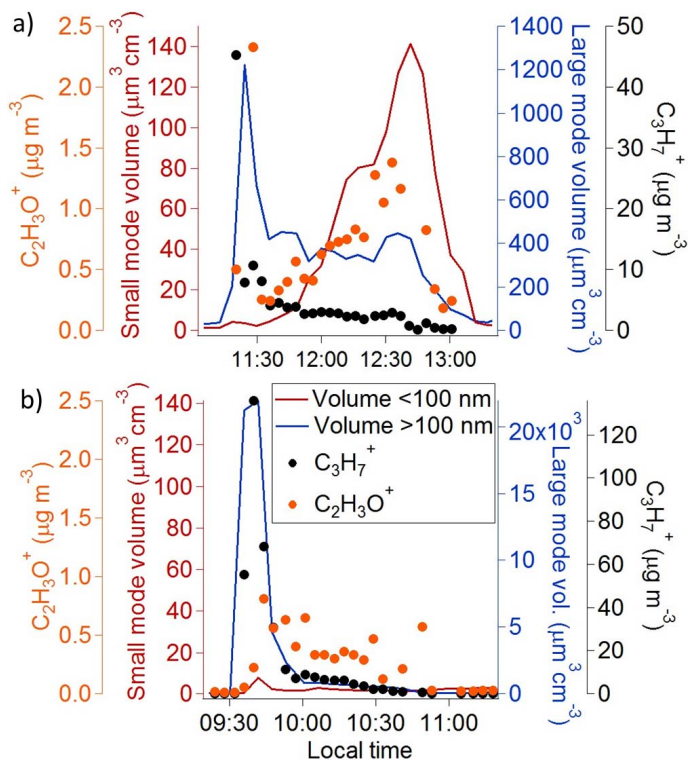
Fig. 10. Volume concentrations in the large (particle diameter > 100 nm) and the small (particle diameter < 100 nm) modes, and concentrations of $C_2H_3O^+$ and $C_3H_7^+$ on 17 July **(a)** and 18 July **(b)**. Total volume concentrations during A2 are comparable on both days. The large mode volume concentration decreases with plume age on both days. On 17 July, the volume concentration in the small mode increases as the plume ages, while on 18 July, no such dramatic increase is observed. $C_2H_3O^+$ covaries with the small particle mode on 17 July, while $C_3H_7^+$ co-varies with the large particle volume on both days.